

Heterogeneous Robot Teams With Unified Perception and Autonomy: How Team CSIRO Data61 Tied for the Top Score at the DARPA Subterranean Challenge

NAVINDA KOTTEGE¹ (Senior Member, IEEE), JASON WILLIAMS¹ (Senior Member, IEEE), BRENDAN TIDD¹, FLETCHER TALBOT¹, RYAN STEINDL¹, MARK COX¹, DENNIS FROUSHEGER¹, THOMAS HINES¹, ALEX PITT¹, BENJAMIN TAM¹ (Member, IEEE), BRETT WOOD¹, LAUREN HANSON¹, KATRINA LO SURDO¹, TEA MOLNAR¹, MATT WILDIE¹, KAZYS STEPANAS¹, GAVIN CATT¹, LACHLAN TYCHSEN-SMITH¹, DEAN PENFOLD¹, LES OVERS¹, MILAD RAMEZANI¹, KASRA KHOSOUSI¹, FARID KENDOUL², GLENN WAGNER², DUNCAN PALMER², JACK MANDERSON², COREY MEDEK², MATTHEW O'BRIEN³, SHENGGANG CHEN³ (Member, IEEE), AND RONALD C. ARKIN³ (Life Fellow, IEEE)

¹CSIRO, Canberra, ACT 2601, Australia

²Emesent, Milton, QLD 4064, Australia

³College of Computing, Georgia Tech, Atlanta, GA 30332 USA

CORRESPONDING AUTHOR: NAVINDA KOTTEGE (navinda.kottege@csiro.au)

This work was supported by the Defence Advance Research Project Agency (DARPA) and the CSIRO.

(Regular Article)

ABSTRACT The Defense Advanced Research Projects Agency (DARPA) Subterranean Challenge (SubT Challenge) was designed for competitors to develop and deploy teams of autonomous robots to explore difficult unknown underground environments. Categorized in to human-made tunnels, underground urban infrastructure, and natural caves, each of these subdomains had many challenging elements for robot perception, locomotion, navigation, and autonomy. These included degraded wireless communication, poor visibility due to smoke, narrow passages and doorways, clutter, uneven ground, slippery and loose terrain, stairs, ledges, overhangs, dripping water, and dynamic obstacles that move to block paths among others. In the final event of this challenge held in September 2021, the course consisted of all three subdomains. The task was for the robot team to perform a scavenger hunt for a number of predefined artifacts within a limited time frame. Only one human supervisor was allowed to communicate with the robots once they were in the course. Points were scored when accurate detections and their locations were communicated back to the scoring server. A total of eight teams competed in the finals held at the Mega Cavern in Louisville, KY, USA. This article describes the systems deployed by Team CSIRO Data61 that tied for the top score and won second place at the event.

INDEX TERMS Multirobot systems, navigation, robotics and automation, simultaneous localization and mapping (SLAM).

I. INTRODUCTION

THERE have been significant advancements in field robotics in the past decade in terms of the maturity of commercially available platforms, advanced sensor technology, navigation capability, power systems, and compute

systems. However, fully autonomous deployment of robots in real-world field applications are still not commonplace. This is especially so in unknown, dangerous, and difficult environments. There seem to be some technology gaps that prevent widespread use of robotic systems in such environments—an

application area that can have significant benefits in removing humans from dull, dirty, and dangerous environments.

Subterranean environments such as mining tunnels, underground urban infrastructure, and natural caves are especially challenging for robots due to lack of global positioning system (GPS) for localization, degraded wireless communication, poor perception due to obscurants, locomotion and navigation difficulties due to narrow passages and doorways, clutter, uneven ground, slippery and loose terrain, stairs, ledges, overhangs, dripping water, and dynamic obstacles that can move to block paths. The Defense Advanced Research Projects Agency (DARPA) Subterranean Challenge (SubT Challenge) was motivated by this gap in technology that was preventing the effective deployment of autonomous robots into this type of environments. As described in [24], the primary scenario centered around providing advanced situational awareness to rescuers following a collapsed mine, earthquake, or personnel lost or injured in a cave. The challenge was designed with extensive input from and in collaboration with first responders. The aims included spurring innovation, building communities of practice, setting new benchmarks for state-of-the-art, and creating societal impact. Point scoring in competition events was achieved by detecting, identifying, and locating an artifact to an accuracy of within 5 m. Artifact classes included survivors (thermal mannequins), backpacks, ropes, helmets, fire extinguishers, power drills, vents, CO₂ concentrations, cell phones, and light emitting diode (LED)-illuminated cubes. To make the scenarios as realistic as possible, the event courses included rough terrain, steep inclines, narrow openings, stairs, water, obscurants such as dust and smoke, and dynamic obstacles (e.g., representing further cave-ins during the mission). Due to the underground environment, GPS is unavailable and communications are severely restricted.

Challenge events commenced with the SubT Integration Exercise (STIX) in the Edgar Experimental Mine, Idaho Springs, CO, USA, in April 2019. The first competitive event was the Tunnel Circuit at the NIOSH Safety Research Coal Mine and Experimental Mine in Pittsburgh, PA, USA, in August 2019. The Urban Circuit event was held in February 2020 at Satsop Business Park, Elma, WA, USA, in an un-commissioned nuclear power plant. The COVID-19 pandemic led to the cancellation of the Cave Circuit event that was scheduled to take place in August 2020. The teams were encouraged to conduct their own testing in local cave environments that they could access. Each year of the challenge represented a Phase, with Phase I including the tunnel circuit, Phase II the urban and cave circuits, and Phase III concluding with the final event. After successfully competing in circuit events in Phases I and II of the DARPA SubT Challenge [13], Team CSIRO Data61 was selected as one of the eight finalists to compete in the final event that was held in September 2021 at the Louisville Mega Cavern, KY, USA (see Fig. 1). After winning the preliminary round at the final event, Team CSIRO Data61 tied for the top score of 23 points with Team



FIGURE 1. Team CSIRO Data61 members at the DARPA SubT Challenge Final Event along with the robot fleet.

CEREBRUS in the final prize run. After tie-breaker rules were invoked, Team CSIRO Data61 won the U.S.\$1 Million second place prize, with only 1 min, 1 cm, or 1 extra artifact report away from first place [7].

This article summarizes the heterogeneous robot system deployed by Team CSIRO Data61, utilizing unified multi-agent mapping and autonomy. We also describe how the team of robots overcame various challenges in the final event course, and the results and lessons learned from the program. The overall system of systems demonstrated remarkable resilience in the harsh environment even in the face of attrition of individual agents. We will focus on the advancements and changes implemented on our systems for Phase III of the competition, in comparison to the work presented in our prior work [13] representing Phases I and II.

A. RELATED WORK

System reviews from the various SubT teams from Phases I and II each contain detailed literature reviews, and can be found in [1], [13], [14], [18], [23], [29], [31], and [37]. Here, we describe the systems employed by SubT teams as described in these papers, and subsequent examinations of particular system components.

Tranzatto et al. [38] described the system employed by Team CERBERUS (University of Nevada, Reno, ETH Zürich, NTNU, University of California Berkeley, Oxford Robotics Institute, Flyability, and Sierra Nevada Corporation) that won first place in the final prize round, with [37] outlining the system from the tunnel and urban circuits. The robot roster for Team CERBERUS consisted of aerial scout uncrewed aerial vehicles (UAVs, including small, medium, and large platforms), a tethered wheeled ground vehicle to extend communications, and two variations of the ANYmal C quadruped: carrier for deploying communication-extender modules, and explorer for proceeding deep into the environment. Graph-based path planning was used with a bifurcated architecture for efficient local and global exploration [8]. Localization and mapping were performed with complementary multimodal sensor fusion (CompSLAM) described by

Khattak et al. [15]. Miki et al. [20] detailed the learning-based perceptive locomotion utilized by the quadrupeds that balance the information from multimodal perception sources to traverse complex terrain (including stairs) in the presence of sensor noise.

Team CoSTAR (NASA Jet Propulsion Laboratory, California Institute of Technology, MIT, KAIST, and Lulea University of Technology) used a combination of Boston Dynamics Spot robots, UAVs, and wheeled robots; the system that was deployed in the tunnel and urban circuits is described in [1]. The focus of their development was networked belief-aware perceptual autonomy (NeBula), which aimed to address challenging, degraded-sensing environments through a combination of sensor fusion, and uncertainty-aware planning. By incorporating map and location uncertainty into the planning problem, risk-aware plans were constructed that account for difficult phenomena such as dust and smoke. Planning under uncertainty is a very challenging problem; this was approached through a hierarchical system described in [16]. The primary modality for simultaneous localization and mapping (SLAM) was lidar/inertial, but alternative solutions were maintained based on visual, thermal, radar, and wheel odometry, fused based on the estimated confidence [30], and used as hints for the lidar/inertial solution [25]. The description of the integration of NeBula onto the Spot-legged platforms to enable autonomous-legged exploration is provided in [3]. A semantic object mapping pipeline provides the operator with enhanced object detections as described in [17].

Team CTU-CRAS-NORLAB (Czech Technological University and Université Laval) solution for the tunnel and urban circuits utilized wheeled Husky UGVs, tracked Absolem UGVs, PhantomX hexapods, and DJI quadrotors [29]. Platforms used various models of lidar, visual cameras, and depth cameras: the Husky used a multibeam lidar and six cameras; the Absolem used a rotating line lidar and a single omnicaera, the PhantomX used RGBD cameras, and the quadrotor used multibeam lidar and cameras. Multiband communications provide high-rate WiFi connection at short ranges (5 and 2.3 GHz), and low-bandwidth control information at longer ranges (900 MHz). Object detection used YOLOv3 trained on 20 000 images, alongside CO₂ and WiFi detection capability. Wheeled and tracked robots used an extended Kalman filter (EKF) to provide initialization for an iterative closest point (ICP)-based odometry method, based on lidar odometry and mapping (LOAM), with no loop closure enabled (since the required accuracy could be met without it). Exploration utilized frontier methods [2], with coordination provided by the human supervisor.

Team Explorer's (Carnegie Mellon University and Oregon State University) system from the tunnel and urban circuit events is described in [31]. Custom wheeled robots enabled coverage of difficult terrain, and the marsupial launch of a UAV. Communications were built around Rajant DX2's,¹

and ground robots carried a total of 24 nodes, which were dropped autonomously based on line of sight and signal strength. Data was selectively shared between robots based on a ledger system. Rather than using a tightly coupled approach, super odometry [43] uses a mixed (loosely and tightly coupled fusion) scheme where visual and lidar inertial odometry (VIO and LIO) estimates are fused with IMU measurements asynchronously to estimate robot trajectory at a fast (200 Hz) rate. Object detection used convolutional neural network (CNN)-based detection pipelines trained on RGB and thermal images, trained using datasets augmented with synthetic data. WiFi and gas localization relied on human interpretation of the noisy signal strengths. The reference coordinate system (i.e., the "gate") was localized using a total station-based calibration. Exploration utilized a hierarchical approach [5], where a global planner maintains a course tour, and a local planner maintains a detailed path within a local region. Exploration was driven by camera coverage of observed surfaces rather than a mapping of 3-D space.

Team MARBLE's (University of Colorado Boulder, University of Colorado Denver, Scientific Systems Company, and University of California Santa Cruz) solution for the tunnel, urban, and cave circuit (held virtually) events utilized map and goal-point sharing among agents [28], a metric-topological graph-based planner and a continuous frontier-based planner [23]. In this system, the base station did not act as a central agent, but instead could relay information as any other agent. In addition, the base station merged artifact reports from all robots, providing the human supervisor with a single submission for detections with a similar position and type. The robot fleet consisted of wheeled Husky and tracked Superdroid UGVs, and Lumenier UAVs. Ground platforms used Ouster multibeam lidars and RGBD cameras with a high-power GPU workstation providing computation, whereas the UAVs used RGBD and ToF cameras. Mapping was performed using Google Cartographer, and map sharing was achieved by extending Octomap to permit the transmission of map differences. Communications were built on custom beacons using a custom transport layer solution named `udp_mesh`.

Team Coordinated Robotics used a teleoperation strategy for the urban circuit event [14]. Due to time constraints in preparing for the event (four months), the team made the decision to focus on integrating multiple platforms with minimal autonomy over a single platform with semi-autonomy. The SLAM algorithm LeGO-LOAM [32] was used, with its output fused with IMU data from two Intel Realsense D435i using the ROS EKF package "robot_localization" [21] for estimating the robot pose and artifact position. As the robots are teleoperated via a video feed, only one robot could be controlled at a time. This led to the team's strategy to use the robots as communication nodes, with a robot teleoperated into the course until the communication bandwidth was unable to sustain the video feed. The robot was then driven back into full communications range using the map data. The next robot was then driven deeper into the course,

¹<https://rajant.com/>

past the previous robot resulting in a wireless communication backbone and data flow to the operator.

Team National Chiao Tung University (NCTU) used a heterogeneous team of ground robots (Husky) and blimps to navigate the complex environments of the tunnel and urban circuit events. An overview of the approach is provided in [18]. Navigation was achieved through deep reinforcement learning (RL) using a cross-modal contrastive learning of representations (CM-CLRs) method, where mmWave radar and lidar data were used for training [11]. Through this approach, the ground robots were able to navigate in smoke-filled environments using only mmWave radar and XBee for communications. The unique aspect of the team's approach was the use of lighter-than-air platforms. The motivation for a blimp was twofold, to enable collision-tolerant navigation and for long-term autonomous flight [12]. With lift achieved by helium, the motors are only required for propulsion, enabling longer flight times. Although the blimp could collide and bounce off the environment, due to the required size of the blimp to generate adequate lift, it had difficulties passing through narrow passageways and was susceptible to airflow within the tunnel. The team attempted to learn a navigation policy for the blimp, but were unable to learn a robust policy due to the inability to model the complex blimp dynamics in the Gazebo simulator.

An in-depth analysis of the results from the SubT Challenge Finals event, along with insights, lessons learned, and future work recommendations were provided in [7]. The performance of the different teams was compared using the competition's singular scoring objective (artifacts detected) as well as describing hypothetical scenarios where the artifact error threshold values (set at 5 m from ground truth for the competition) were adjusted. Alternate relevant evaluation metrics, such as lowest map deviation, greatest map coverage, largest map (points), and fastest successful report, were also introduced to compare the teams' solutions. In addition, technical and operational insights based on the competition results and the evolution of technology during the Challenge period were provided. The most successful solutions had a heterogeneous team (different platform mobility and function) of robots built upon reliable commercial-off-the-shelf (COTS) products. This allowed the solution to adapt to different scenarios and reduce the impact when attrition of robots occurred. Another insight provided was on the crucial role the human supervisor performs. While the human supervisor was a mission enabler, providing high-level commands and coordination, they were also the weak link, where the cognitive load of the human supervisor could limit performance.

B. CONTRIBUTIONS

The key differentiator in our solution is the homogeneous sensing capability, which enables shared maps between all agents. UGVs and UAVs both utilize spinning lidars which power both mapping and autonomy, with cameras providing object detection capability. The highly modular UGV

solution centered around a common sensing pack and navigation stack has enabled rapid adaption to a wide range of platforms. All agents utilize the same SLAM system, which develops complete shared maps on each agent. These were exploited to provide shared global maps between all ground agents, and multirobot task allocation.

This article includes a brief description of our full system approach, with further detail on aspects that changed from our Phases I and II system described in [13]. Further details of the earlier work can be found in [13]; particular differences from this approach include the following aspects.

- 1) The UGV exploration system was revised to calculate traversability frontiers, utilizing multiagent global mapping data.
- 2) A new planner was developed that specifically targeted passing through narrow gaps.
- 3) The multirobot task allocation reward function was reformulated to incorporate elements that consider the positioning of all agents in the tunnel network.
- 4) The tools available to the human supervisor for prioritizing tasks and altering assignments were greatly improved.
- 5) The object tracker was redeveloped to associate new detections to full multirobot histories (as opposed to a recent window on the local agent).
- 6) The Boston Dynamics Spot was incorporated into our robot fleet, and integrated with our common sensing and autonomy stacks.
- 7) The drop nodes and dropping mechanisms were redesigned based on lessons in prior events.
- 8) A new UAV platform was adopted to overcome the limitations of the previous platform, and hardware was integrated to permit the use of the same object detection pipeline as ground agents.
- 9) SLAM was modified to selectively share frames, avoiding repeated sharing of identical frames when the robot is not moving significantly.

In addition, we describe in detail, the results of the approach at the final event of the DARPA SubT Challenge.

- 1) For each run, details of the operator's intentions, complicating events, and results.
- 2) Communications performance, use of autonomy and human intervention.
- 3) Object detection performance and lessons learned.
- 4) Analysis of the mapping performance achieved in comparison with the ground truth scans provided by DARPA.
- 5) Experiences providing remote support due to severe limitations on the deployed team.

II. SYSTEM DESCRIPTION

SubT involves a fleet of robots autonomously exploring an underground environment under the control of a single human supervisor. The final event combines the challenging elements from tunnel (e.g., large scale), urban (e.g., stairs), and cave (e.g., extreme terrain) environments. The solution

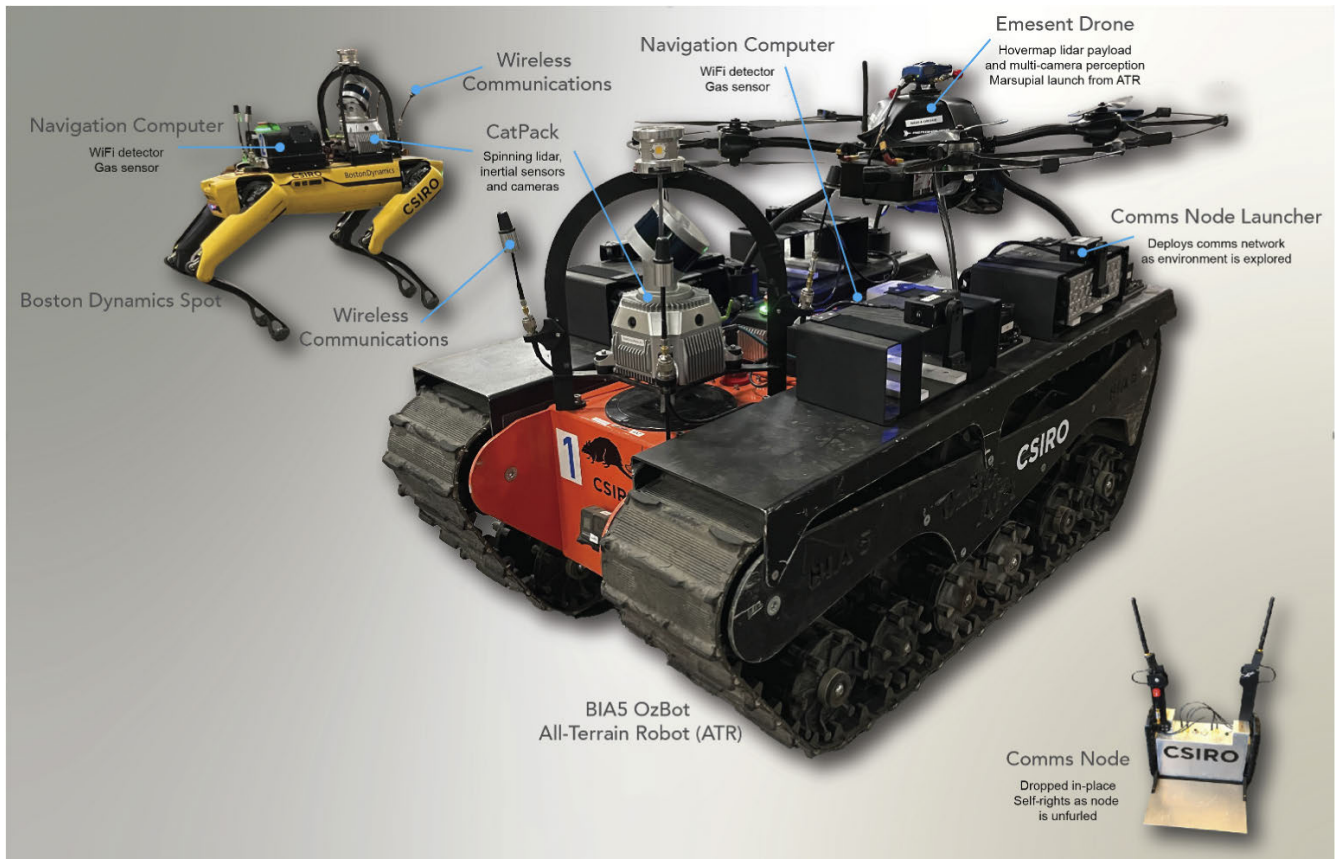


FIGURE 2. Team CSIRO Data61's robot platforms deployed during the final event.

fielded by Team CSIRO Data61 at the final event involved two Boston Dynamics Spot robots,² two BIA5 OzBot all-terrain robots (ATRs),³ and two Emesent UAVs carried by the ATRs. Communications nodes based on the Rajant Breadcrumb ES1 were carried on the ATRs and deployed through the course. The fleet employed is illustrated in Fig. 2.

In this section, we describe the hardware components of the system. We begin in Section II-A describing the UGV platforms developed for the final event, and subsequently the UAV system in Section II-B. Finally, Section II-C describes the design of the communications system.

A. UGV PLATFORMS

The hardware systems architecture for the UGV platforms is summarized in Fig. 3. A number of minor changes were made to the architecture deployed in the earlier phases of the SubT Challenge. The primary change to Fig. 3 is the addition of the Boston Dynamics Spot and the removal of a universal serial bus (USB) hub connecting external sensors. These changes and modifications are described in Sections II-A1–II-A3.

1) BIA5 OzBot ALL-TERRAIN ROBOT

The BIA5 OzBot ATR was first utilized by Team CSIRO Data61 in the tunnel circuit event in August 2019. Subsequently, a lightweight (90 versus 300 kg) version was custom-built for CSIRO by BIA5 and employed in the Urban Circuit event and cave testing performed in lieu of the cave circuit event.

The same robots were utilized in the final event, using the same LiFePO₄ batteries, power system, and Cincoze DX-1100 ruggedized workstation (with Intel i7-8700T CPU). An evolved version of the “CatPack” perception pack was utilized, providing lidar, IMU, and cameras with integrated compute performing SLAM and object detection. The new CatPack version had a fully machined aluminum housing instead of the previously mixed aluminum and printed plastic housing, providing better dust and moisture protection, more effective cooling, and better camera lens mounting giving improved image focus. A WiFi and Bluetooth module was also integrated into the CatPack and could be used for artifact detection instead of USB-connected modules.

Extensive improvements were made to the robot's motors and motor controllers. The motivation for this was twofold; first, to overcome issues with burn-out of motors in autonomous operation; and second, to provide finer control over the paths that the robot executed. The changes made are

²<https://www.bostondynamics.com/products/spot>

³<https://bia5.com/>

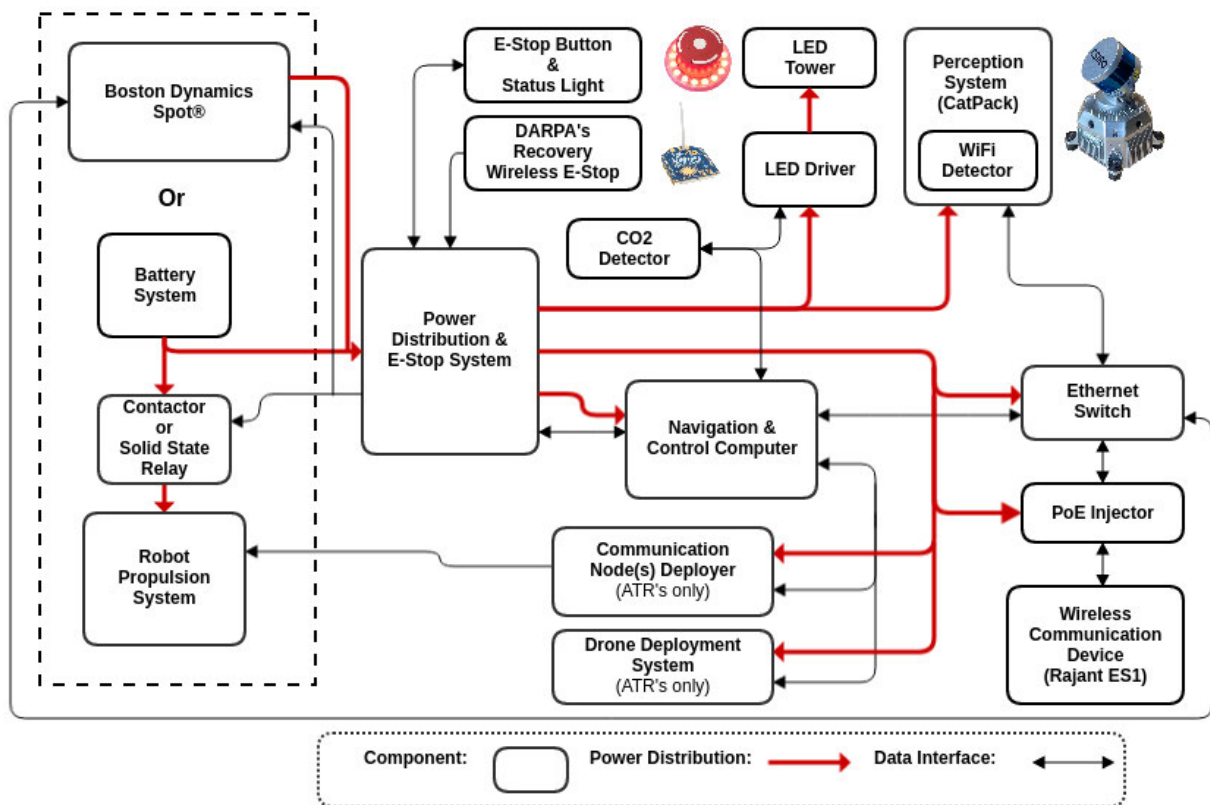


FIGURE 3. Hardware systems architecture for the Spot, DTR, and ATR platforms.

representative of those that have been found to be necessary to support autonomous operation on other platforms designed for teleoperation. The platform speed is 1.2 ms^{-1} .

In relation to robustness, motors were burned out on a number of occasions. The first instance of this occurred during the Urban Circuit event, where a track became fixed on a large hook concreted into the ground. Subsequently, additional burn-outs occurred on a number of occasions where one track lost traction and spun repeatedly as autonomy attempted to recover from the condition. This was addressed first by introducing higher torque motors (a custom 108 mm out-runner motor configuration coupled with BIA5's gearboxes) that were capable of handling more heat, and second by upgrading the motor control system and introducing a thermal model of the motor. The upgraded motor controller used an Elmo motion control (MC) system, providing feedback on current, temperature, velocity, and acceleration at 200 Hz.

The thermal modeling introduced to this system was used to estimate the core temperature of the motor from an externally mounted thermistor on the motor casing. The thermal transfer from the motor core to the casing was based on a model provided by the motor manufacturer [19]. On each update of the motor communications loop, the motor current and thermistor readings would be fed into the model to get an internal temperature estimate. This allowed the system to apply significantly more power to the tracks in short bursts

without risking a burnout, and consequently increasing the overall agility of the platform.

In relation to fine motor control, the stock motors and controllers had a range of difficulties, such as low-rate feedback (10 Hz), simple proportional, integral, derivative (PID)-based control, fixed acceleration limits, and an opaque interface. Most significant among these was the PID-based control, which resulted in a significant overshoot due to a large integral wind-up to overcome stiction. This presented a significant barrier in tight environments such as when navigating through a narrow doorway. In contrast, the Elmo MC's built-in system identification was utilized to obtain precise velocity control. The higher bandwidth 200-Hz feedback also enabled improvements to the outer control loop, which was executed over a dedicated Ethercat interface. This higher rate feedback was utilized to implement a differential drive controller which balanced the desired level of aggressive control with smoothing when excessive velocity changes were commanded (e.g., when switching to a time-critical recovery behavior).

Our efforts provided us with a highly robust platform capable of aggressive navigation, yet with exceptional fine control. This platform demonstrated robust control in adversarial terrain conditions in testing such as large rock piles and stairs, as well as challenging deformable cave environments in the self-led cave circuit. Around the time of the final event, further motor replacements were required, but these

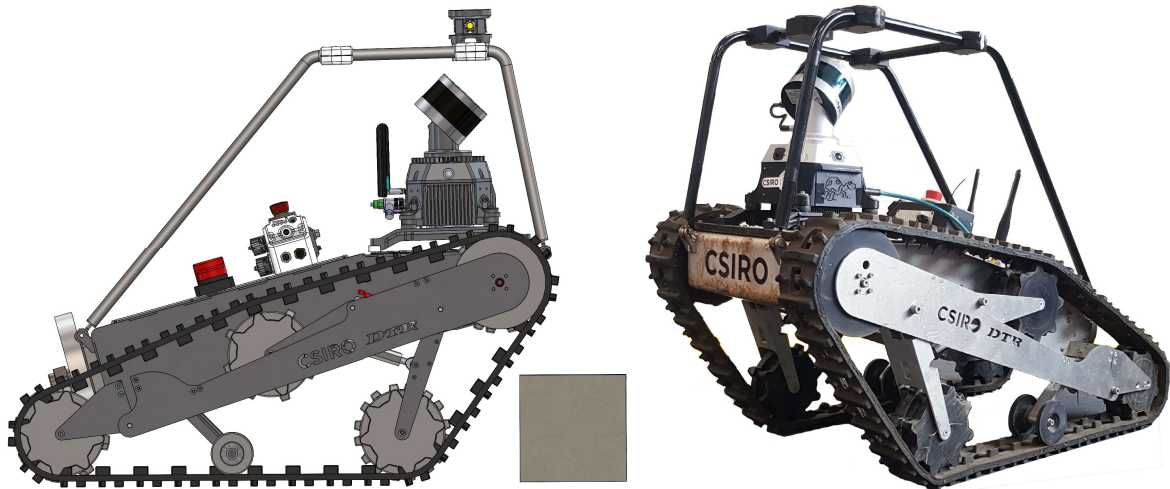


FIGURE 4. New DTR design showing its improved obstacle clearance ability next to a 180 mm high step in a CAD diagram (left), and the real robot carrying an earlier version of the CatPack perception pack (right).

appeared to be related to deterioration over time rather than particular traumatic events. We plan to address this in future design iterations through an integrated gearbox, motor, and controller solution.

2) CSIRO DYNAMIC TRACKED ROBOT (DTR)

The CSIRO DTR was developed to combine the strengths of the ATR with those of the smaller SuperDroid LT2-F, particularly around stairs and narrow doorways. Development of this platform continued from its initial design used at the self-led cave circuit up to the final event. Mechanically, the track tension mechanism was improved by coupling the position of the tensioner wheel and suspension arm. Their coupled motion maintains a constant tension in the track throughout the motion range of the suspension arm. This maintained soft suspension, but achieved the high track tension needed to provide robustness to small rocks in the tracks. The final design of the platform is shown in Fig. 4; the platform is capable of operating at a speed of 3 ms^{-1} , but is configured to use a similar speed to the ATR due to the tuning of autonomy.

The design maximized commonality with the ATR components, and served as a prototype of the Elmo MC system described in Section II-A1. This commonality was an explicit design goal, to permit either platform to provide spare parts for the other. The same CatPack perception was utilized as the ATR, while the navigation computer was based on an Intel NUC NUC8i7BEH.

Tuning of the autonomy stack for the DTR was de-prioritized when the Spot was integrated into the robot team, but continued at a low rate of effort. It was intended that the platform would feature in the team at the final event, but this needed to be dropped due to the minimal team that was able to be sent due to COVID-19 travel restrictions. An accurate simulation model of the platform was developed, and was utilized by Team CTU-CRAS in the DARPA SubT Challenge Virtual track. The platform is seeing continued use,

particularly in natural environments where it has less impact than the larger and heavier ATR platform.

3) BOSTON DYNAMICS SPOT QUADRUPED ROBOT

The Boston Dynamics Spot platform is a COTS quadrupedal-legged platform. It features a top speed of 1.6 ms^{-1} , a max payload of 14 kg, and a typical operation time of 90 min (unloaded; typical operation times were 40–45 min with a payload). It has stereo cameras positioned around the body which allow it to generate a 360° map of the local terrain. This map, combined with state-of-the-art locomotion software, allows it to traverse a wide array of terrain. The Spot platform was used to navigate into areas that were unsuitable for the tracked ground platforms, including stairs, and narrow passageways [35].

Previously the Ghost Robotics Vision60 Platform had been fulfilling this role within the fleet. The decision to switch to the Spot platform was made based on testing its performance in these specific areas. Predominant capabilities of the Spot are understood to be due to its terrain sensing: Unlike the Spot platform, the version 4.2 Vision60 platform available at the time did not provide any local terrain mapping or foothold planning, which made it unsuitable for traversing stairs, a key area the legged platform was aimed at addressing. The Spot platform also provided a payload interface that was more robust, better documented, and supported for the user. This not only allowed the team to rapidly integrate Spot into the fleet, but also allowed the onboard sensor data to be integrated into the team's autonomy stack as described in Section IV-A4.

As illustrated in Fig. 2, the Spot was fit with the same CatPack perception pack utilized in the other platforms, along with the same navigation computer utilized with the DTR and the earlier Ghost platform. Communications were provided by a Rajant ES1 Breadcrumb node as detailed in Section II-C, however, the platform was not equipped to drop additional nodes.

B. UAV PLATFORM

The SubTerra “Navi”⁴ UAV used in the SubT Finals is the first UAV specifically designed to work with the Emesent Hovermap payload with specifications given in Table 1 (see Fig. 5). This platform was commissioned from the New Zealand-based company, Aeronavics, by Emesent.

Throughout all previous circuits, our UAV platform of choice was the DJI M210. Whilst this platform was robust and met our size and payload requirements, it provided some challenges when pushed beyond its manufacturer-expected use cases. Most critical were random events in which the UAV would override take-off commands due to perceived magnetic interference. The act of moving an ATR through a circuit with an M210 on the back could cause sufficient interference with the UAVs in-built sensors, raising an error. A further problem was that, once fully loaded with the Hovermap, communications node, and vision system, it only provided around 8 min of flight time. With these problems in mind, a fully configurable platform with a 20-min battery life, and high payload capacity was required to allow for full control over every aspect of the system and achieve our desired coverage goals.

With no commercially available UAVs on the market at the time, Emesent commissioned a custom solution from Aeronavics based on their existing Navi UAV. The Navi provided an Ardupilot-based system that met our transparency, flight time, and lift capacity requirements. Unfortunately, the development of this platform was problematic requiring significant effort to improve platform reliability. Such reliability issues included electronic speed controller (ESC) burnout, debris ingress through open motor housings, battery failure, short life-span, and communications issues with the ground station remote controller (RC). Ultimately, most of these problems were solved or mitigated before the final circuit and the platform proved itself. In the second preliminary round, one Navi platform was downed by a sheet of foam in mid-air, however, the system sustained no major damage to the air-frame, Hovermap, or vision system, only requiring prop replacement to be back in the air within an hour of returning to the pit.

A feature of this platform was propeller guards. These were installed when needed as they traded increased survivability in the air for reduced ability to enter narrow passageways while riding the parent vehicle. Whilst on the ATR, the propeller guards extended beyond the UGV’s 780 mm width, preventing the ATR from entering as narrow passages. The guards also increased the UAV’s width in flight, but the UAV could still navigate the same size tunnel, as light contact with the wall would no longer guarantee a crash. In the final circuit, propeller guards were installed for the first preliminary run to ensure that the UAVs would return intact. For the second and final runs, a more risky approach was taken and guards were removed from all UAV systems.

TABLE 1. UAV specifications—loaded with Hovermap and vision system.

Property	Value
Length	740 mm
Length (With propeller guards)	900 mm
Width	740 mm
Width (With propeller guards)	900 mm
Height	350 mm
Weight	5.8 kg
Nominal clearance from robot center	850 mm
Minimum passage width	2000 mm
Minimum take-off clearance	1000 mm
Flight time (Fully Loaded)	20 min
Nominal movement speed	1.5 ms ⁻¹
Maximum movement speed	2.0 ms ⁻¹

1) UAV VISION SYSTEM

Accompanying the Navi platform was a new vision system called the “Tick” (see Fig. 6), which was developed in parallel with improvements to the previous gimbal-based approach before being chosen as the UAV vision system for the final circuit. Specifications of the Tick are given in Table 2.

Prior to the tick, a gimbal-based vision system was employed by our UAVs. This was an in-house design utilizing off-the-shelf electronics to create a fully controllable and stabilized gimbal. A single FLIR BFS USB 3.0 camera would feed frames through the Hovermap to an Intel Neural Compute Stick 2 for image classification. This secondary compute unit was required as on-board image classification would compete with SLAM, trajectory planning, and other core processes for CPU resources, leading to higher image classification latency and a lower output rate.

The gimballed camera system, along with our visual coverage tracking software, could scan the course independently of UAV orientation. Compared to a static system, this provided enhanced vertical coverage of the course and a higher chance to detect objects when the platform was stationary. In theory, the single moving camera with a narrow-moderate field of view (FOV) allowed for both highly detailed images at long ranges and large field coverage given enough time in one region. However, due to the limited flight time of small UAV platforms, it was not practical to loiter in one region for extended periods, thus in prior SubT circuits it suffered from limited coverage and missed target objects.

Due to these coverage limitations, we developed a static, multicamera system with on-board processing utilizing CSIRO Data61’s perception stack. As the Hovermap host system was used to run the Wildcat SLAM solution, this package could leverage smaller NVIDIA Jetson hardware than the CatPack used on the UGV. This system was called the Tick due to its parasitic nature on the Hovermap.

At its core, the Tick ran an NVIDIA Jetson Xavier-NX on a connect-tech quark carrier board, allowing for dual

⁴<https://aeronavics.com/models-of-drones/navi/>



FIGURE 5. Emesent/Aeronavics SubTerra (“Navi”) UAV (left), being launched off the back of an ATR UGV (center), and in flight inside the DARPA SubT finals course (right).

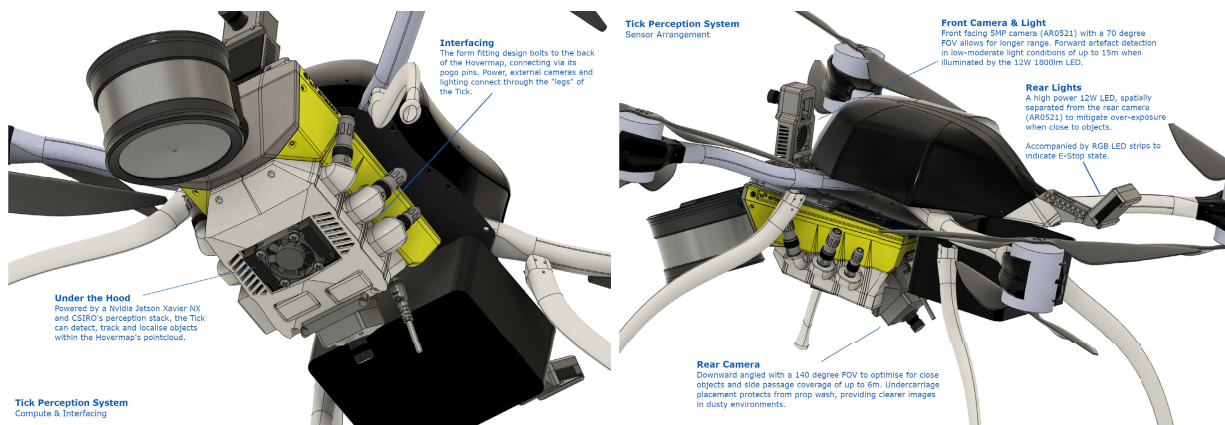


FIGURE 6. Anatomy of the vision system (the tick) on an Emesent Navi UAV showing compute and interfacing (left) and sensor arrangement (right).

MIPI-CSI cameras. Whilst the Xavier-NX had the connectivity and processing power required to run more cameras, carrier board and weight restrictions limited this to two cameras. The specific camera arrangement and lens combination were the single largest factor in the performance of the tick. Initially, the tick was configured with dual downward angled, forward/side facing, wide FOV (160° – 180°) cameras to maximize coverage, with particular focus on the space directly in front of the UAV and that of unexplored pathways/nooks to either side. Testing showed that this configuration suffered from problems as follows.

- 1) A short range of only 5–6 m due to the large FOV of each camera.
- 2) High power consumption due to the lighting requirements for such a large FOV.
- 3) Over-exposure of the image due to reflections from UAV legs.
- 4) After transitioning from the M210 to the Navi, the new leg setup with four legs placed at the UAV corners blocked a significant part of the camera FOV.

Further testing led to the final configuration, consisting of one front-facing, 70° FOV camera, and one rear, downward-facing 140° FOV camera. This configuration was able to maximize both the system’s coverage and range by relying on the tendency of the exploration code to stop and spin in place when passing an unexplored passageway. The rotation of the platform allowed the fixed cameras to cover a larger FOV, with the board FOV (140°) sensor specializing in targets close to the UAV (~ 5 – 8 m), while the narrow FOV camera could search for targets at ranges of up to 15 m. Continued improvements to the system included aspects of the lighting configuration. Specifically, increasing vertical separation between the rear lights and camera significantly reduced image blow-out on close objects and increased the accuracy of the tick.

C. COMMUNICATIONS SYSTEM

The communications system used in the final event closely matched the solution that was deployed at the urban and cave events. COTS Rajant Breadcrumb nodes were used to provide

TABLE 2. Tick specifications.

Property	Value
Camera Sensor	AR0521
Camera Resolution	5.1 MP
Camera Frame-rate	3 FPS
Front Camera FOV	70°
Front Camera Maximum Artefact Range	15 m
Rear Camera FOV	140°
Rear Camera Maximum Artefact Range	6 m
LED Power	12 W + 12 W
LED Luminous Flux	1800lm
Total System Power Consumption	45 W

a layer 2 (i.e., the data link layer in the OSI communications model [44]) mesh network using wireless, dual-band (2.4 and 5.8 GHz) 802.11 radio links. The base station and robot autonomy computers all used a standard Linux TCP/IP stack to communicate over this network. Layer 4 (transport layer) traffic was handled exclusively by a software component named Mule, described in Section II-C4.

1) BASE STATION COMMUNICATIONS

The base station computer was connected to two Rajant Breadcrumb nodes: an ES1 and a Peregrine. Each node was mounted with antennae on dedicated masts that provided approximately 1.5 m of ground clearance. The ES1 was connected to 4 dBi (2.4 and 5.8 GHz), multipolarized, omnidirectional, goose-neck style antennae whilst the Peregrine was connected to 9 dBi (2.4 GHz) and 12 dBi (5.8 GHz), directional sector antennae. The decision to use multiple node masts at the base station was made during the lead-up to the event and was motivated by the idea that the course entrance may have consisted of two or more narrow tunnels which would not be well handled by a single directional antennae. Though the actual course used a single entrance tunnel, the team decided to continue deploying both mast nodes in each run due to early results indicating a nonnegligible degree of RF transparency through some of the course walls.

2) COMMUNICATIONS NODE DROPPING MECHANISM

Whereas the earlier communications node design was a minor repackaging incorporating a battery into the Rajant Breadcrumb ES1, the node utilized in the final event underwent a major redesign. The core ES1 node was supplemented by a Raspberry Pi 4, which served two functions. First, it controlled the deployment of the node. Rather than being statically dropped, the revised node design actively unfurls two side panels, self-righting in the process, powered by Dynamixel motors. Subsequently, antennae unfurl to a configuration with sufficient height to provide improved communications quality, and finally, the ES1 power is activated. The deployment process and design are shown in Fig. 7.

The Raspberry Pi 4 also provided the secondary capability of running an instance of the Mule communications software on the node. Due to the reprioritization of tasks in the lead-up to the final event (again, due to COVID-19-related travel restrictions for the team), insufficient experimentation had been conducted with this concept prior to the final event, so the capability was not employed. However, it has the potential to allow nodes at the boundary of communication to retain data from a robot as it goes deep beyond communication.

The node dropper design also evolved for the final event. Lessons from testing in the cave environment showed that carrying node droppers which extruded beyond the vehicle footprint was highly undesirable. It was also found that dropping to the side of the platform was preferable over dropping in front or behind, as it inherently tended to result in node positions which did not block the traversal of a passage. Accordingly, as shown in Fig. 2, four-node droppers were installed on the track guards of each ATR (two on each side).

3) UGV AND UAV COMMUNICATIONS SYSTEM

Each UGV was equipped with a Rajant ES1 node connected to 4 dBi (2.4 and 5.8 GHz), multipolarized, omnidirectional, goose-neck style antennae. Each UAV was equipped with the smaller Rajant DX2 node connected to 2.6 dBi (5.8 GHz only), omnidirectional, lollipop-style antennae due to size and weight constraints.

4) MULE

Mule was the layer 4 software component which bridged ROS topic messages between the independent ROS systems running at the base station and on each robot. Mule provided best-effort, end-to-end transport for ephemeral data such as robot status and teleoperation video, as well as disruption-tolerant, hop-by-hop transport for mission-critical data such as Wildcat frames, and object detection reports. These features enabled the operator and autonomy software to use data-muling as a strategy for improving exploration efficiency and overcoming robot attrition.

Improvements were made to the design of Mule for deployment in the final to expose more information to the human-operator, such as providing more detailed information on exactly what data was yet to be downloaded from a given peer, and a separation of “synchronization lag” into upload vs download metrics.

The capability provided by Mule was critical to the outcome achieved at the final event. For example, as described in Section VII, in the final prize run, data from a fallen Spot robot was relayed to another platform that passed nearby, and later transmitted to the base. It was these data-muling efforts that resulted in the final successful artifact report in the final critical seconds of the run.

5) COMMUNICATION SYSTEM IMPROVEMENTS

Despite the core design of the communications system remaining relatively unchanged between the urban and final events, significant performance improvements were attained

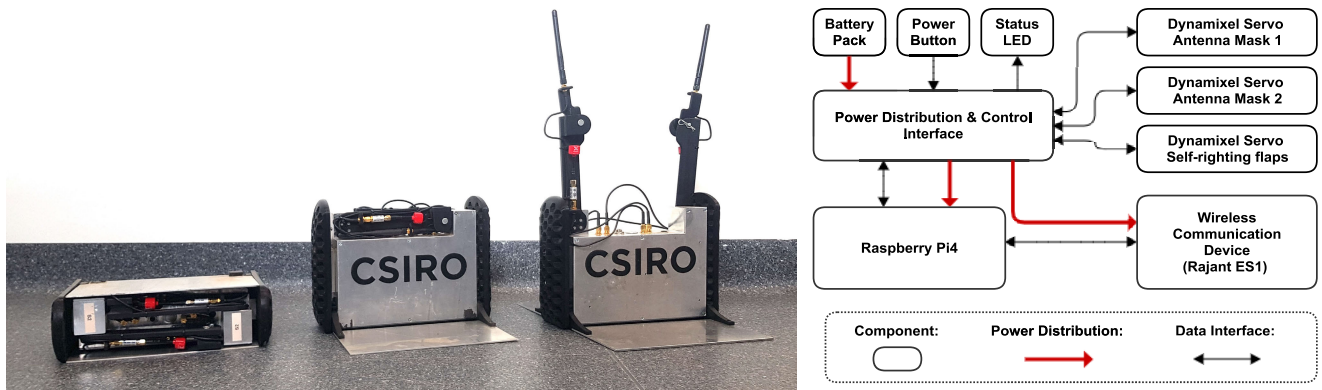


FIGURE 7. (Left) Communications node packing, showing stages of deployment: as dropped from the robot, after side panels unfurl, self-righting the node, and after antenna deployment. (Right) Block diagram of communications node design.

due to the resolution of previously undiscovered integration issues.

The first of these issues was related to the active Bluetooth scanning being used for the detection of the mobile phone artifact. At the Urban event, UGVs were equipped with a UD100 Bluetooth USB adapter and software that would repeatedly perform active Bluetooth “inquiry” scans to elicit responses from nearby Bluetooth devices. Each of these scans involved brief transmissions on a sequence of 1-MHz Bluetooth channels spread across the 2.4-GHz ISM band. These transmissions were unmanaged with respect to the 20-MHz 802.11 channel that was used by Rajant Breadcrumbs in the same 2.4-GHz ISM band. Integration testing conducted after the Urban event revealed that these Bluetooth transmissions were significantly degrading the performance of the Rajant mesh network. With consideration of overall system performance and time constraints, it was decided that the Bluetooth detection capability would be removed from UGVs altogether, relying on (passive) WiFi detection (for cell phones) and the visual signature of the cube artifact. A similar 2.4-GHz interference problem was discovered with the RC transceiver, however, this scenario was restricted to times when the handheld RC unit was switched on and in close range of the robot (a situation that could not arise during actual competition).

The second of these issues was related to unintentional mesh network traffic originating from devices other than the base station and autonomy computers. The hardware designs of the UGVs and UAVs both contained a single Ethernet network that was used to connect the robot autonomy computer with on-board sensors, controllers, and the Rajant Breadcrumb node. Early on in the development process, the Rajant Breadcrumb nodes were configured to use a bridging mode where layer 2 packets received via the local Ethernet connection could be transported via the mesh network regardless of the source address. This configuration simplified certain aspects of system development by allowing access to network-enabled robot hardware from any computer connected to a Rajant Breadcrumb. However, this configuration

left the performance of the communications system vulnerable to unexpected sources of network traffic. Such sources were inadvertently introduced on multiple occasions during development. On each occasion, a new piece of hardware had been introduced that defaulted to a communication mode that generated a high-frequency stream of packets with a layer 2 broadcast destination address. This would result in a subtle but significant degradation of the communications system performance during subsequent system tests, requiring manual traffic analysis to detect and identify the offending hardware. Prior to the final event, it was decided that the Rajant Breadcrumbs would be configured to use a MAC address whitelist so that only layer 2 packets originating from the base station and robot autonomy computers could be bridged over the mesh network.

III. LOCALIZATION AND MAPPING

Robust localization and mapping are critical to downstream robotics tasks. For example, as described in Section IV, robot autonomy requires the information of localization and the environment map for path planning, multiagent coordination requires knowledge of each robot’s position on a shared map, and in SubT, detected artifacts must be reported with accurate locations. This section briefly describes Wildcat, our multi-agent lidar-inertial SLAM system used in the DARPA SubT Challenge. We refer the reader to [27] for additional technical and implementation details. A consolidated report on the experiences of the various SubT teams with localization and mapping can be found in [9].

A. WILDCAT SLAM

A diagram of Wildcat is shown in Fig. 8. Wildcat has two major modules: 1) lidar-inertial odometry and 2) pose-graph optimization (PGO). In the following, we briefly describe each module and present our SLAM results in the prize run of the DARPA SubT Challenge Final Event.

Wildcat odometry is a real-time sliding-window optimization method that fuses IMU and lidar measurements collected within a 3-s window to estimate robot trajectory at a high

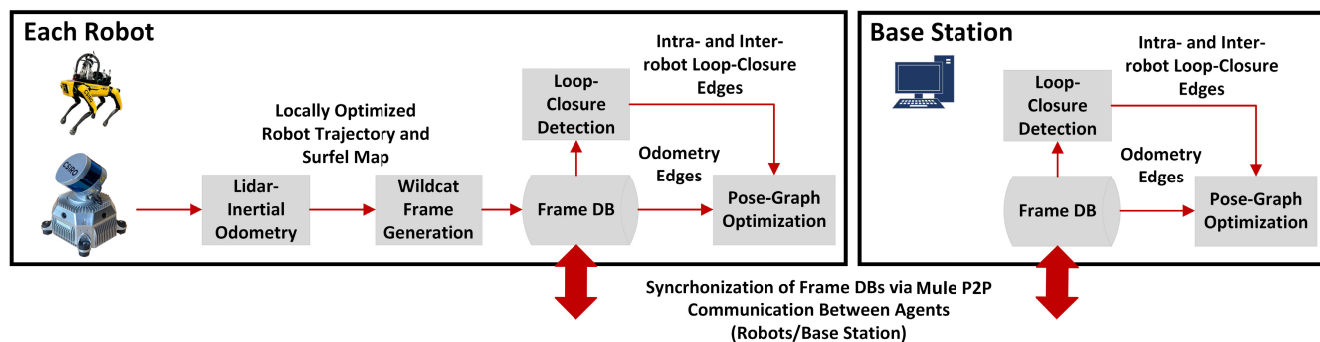


FIGURE 8. Diagram of Wildcat, our multiagent lidar-inertial SLAM system. This diagram shows the components of Wildcat ran on each robot (left) and those that ran on the base station (right).

rate. The odometry module runs on each robot independently. First, Wildcat generates surfels from lidar points by voxelizing them and fitting an ellipsoid to the points residing in each voxel. Only those surfels that are sufficiently planar are kept.

After establishing an initial set of correspondences between the surfels, Wildcat then estimates robot trajectory by minimizing the point-to-plane distance between the matched surfel pairs and also the error between the predicted and collected IMU measurements (angular velocity and linear acceleration). Wildcat odometry alternates between matching surfels and estimating robot trajectory for a fixed number of iterations. Our method uses cubic B-spline interpolation to remove distortion from lidar points (caused by the motion of the robot and lidar) and to efficiently fuse asynchronous measurements from lidar and IMU in the previously mentioned optimization problem; see [27].

Every 5 s, the locally optimized robot trajectory is used to create a local surfel map. We call each rigid local map (together with additional information such as the corresponding segment of trajectory estimate) a *frame*. Frames remain rigid after creation and thus their state can be represented by one of the underlying poses. Each robot stores its own frames, as well as frames received from other robots in a database. Frame databases are synchronized between the agents (robots and the base station) using Mule whenever peer-to-peer communication is possible (see Section II-C4); frames are suppressed from being shared if the overlap to the previously shared frame exceeds a threshold. Wildcat’s PGO module (also referred to as Atlas) runs separately on each agent and aims to produce an independent, globally consistent estimate of the team’s map and trajectories. This module detects intrarobot and interrobot loop closures using all available frames. Each agent then independently optimizes the team’s collective pose graph whose nodes correspond to (unknown) frames’ representative poses, and whose edges correspond to odometry and loop-closure measurements. In the prize run, the average total size of frames generated by our four UGVs (introduced in Section II-A) was about 21.5 MB per robot.

Fig. 9 shows the map created collaboratively by our robots by the end of the prize run. According to DARPA, this

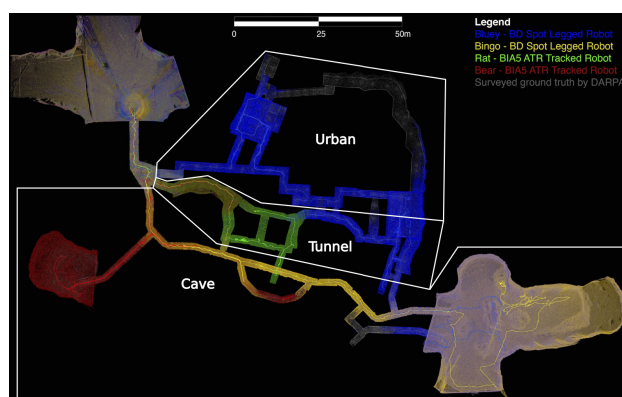


FIGURE 9. Multiagent globally optimized Wildcat SLAM map from the robots deployed by team CSIRO Data61 during the 60-min prize run. Point clouds collected by different robots are shown by color, while white lines delineate the three-course environments (i.e., urban, tunnel, and cave).

map has “0% deviation” from the surveyed ground truth where “deviation percentage” is defined as the percentage of points that are further than one meter from the surveyed point cloud.⁵ Fig. 10 shows the maps created by all teams by the end of the prize run. Green (respectively, orange) points correspond to map points whose distance from the surveyed point cloud is less (respectively, more) than 1 m. Our team produced the most accurate map at the final event, while also having “91% coverage” according to DARPA. We conducted our own quantitative analysis using the surveyed point cloud map provided by DARPA in [27]; the results show that the average distance between our map points and the nearest point in the reference map (after aligning the two maps) is about 3 cm.

Moreover, Fig. 11 depicts the collective pose graph based on one of the agents during the prize run. In total, 3950 frames (gray nodes) were shared between four agents out of which only 49 nodes were considered as root nodes (green nodes) whose poses were estimated through the pose graph optimization. If frames sufficiently overlapped with a

⁵<https://www.youtube.com/watch?v=SyjeIGCHnrU&t=1932s>

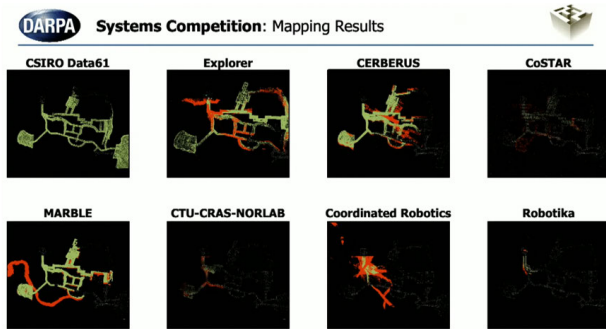


FIGURE 10. Visual comparison of online mapping data reported to DARPA during the competition runs for the eight finalist teams during the final prize run, with points matching ground truth shown in green, and nonmatching points shown in orange. *<https://youtu.be/SyjeIGCHnrU?t=1676>

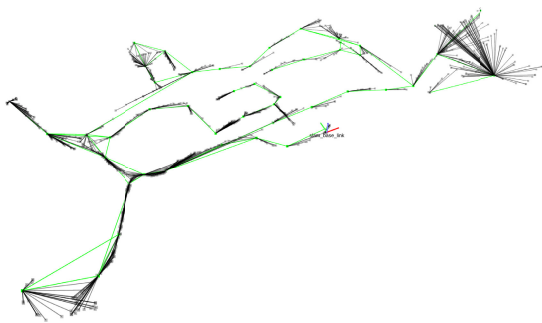


FIGURE 11. Pose-graph collected from four agents on one of the agents whose location is indicated by the red and green coordinate frame, during frame sharing. The white lines represent the connectivity between the children frames whereas the green lines indicate the connectivity between root nodes.

root node, they are considered as child nodes and they are rigid relative to the root node. This strategy decreases the number of root nodes as a result the number of parameters in the pose graph optimization allowing Wildcat to deal with scalability in an efficient manner.

IV. AUTONOMY

Autonomy is critical in SubT due to the dual limitations of a single human supervisor, and the communications challenges of underground environments. This section describes the solution utilized for this. For UGVs, we first describe the local autonomy in Section IV-A, then the global autonomy in Section IV-B, and finally the multirobot task allocation in Section IV-C. Subsequently, we describe the UAV autonomy in Section IV-D.

Block diagrams of the respective UGV and UAV autonomy systems are shown in Fig. 12. The key component in common between the two is the Wildcat SLAM system, described in Section III-A.

A. UGV LOCAL AUTONOMY

The Wildcat SLAM system, described in Section III-A, is a key underpinning technology to the solution. Local

navigation primarily utilizes the point cloud provided by the Wildcat odometry process. This is integrated into a 3-D GPU-based occupancy map through the GPU-based occupancy homogeneous map (OHM) system, detailed in [34]. The occupancy grid is populated to a minimum range of 10 m (with discrete jumps due to region-based addressing), and a resolution of 0.1 m. Height maps are extracted from the OHM grid. Support was included for multiple vertical layers in height maps, e.g., to support navigation up a staircase in an area where the region beneath the staircase is also visible, but this remained to be fully utilized in the downstream parts of the stack at the time of the competition. The height maps include awareness of the clearance height required by the respective platform, and so will not output a ground level beneath an overhang with insufficient clearance.

As described in [10], an important feature of the height map generation is the identification of *virtual surfaces*. These represent horizontal frontiers, where the space above has been identified as free space, but the space below is unknown. Consequently, they are surfaces that have not been directly observed, but observed data implies the potential presence of a surface beneath. The navigation stack utilizes this by initially treating them as traversable, so that the agent will move toward them and either observe the surface itself, or identify the fatal incline descending from the top edge, as illustrated in Fig. 13.

Traversability is assessed using the height map at two different ranges and rates. Local traversability analyses terrain at a shorter range (4 m) but at a higher rate (5 Hz), whereas global traversability analyses terrain at a longer range (6 m) but at a lower rate (1 Hz). The traversability analysis consists of tests on slope and steps. The slope analysis considers hypothetical (circular) robot footprints at each location in the map, and evaluates the resulting attitude. The cell is considered fatal if the slope exceeds a threshold. The step analysis searches for discrete steps exceeding a threshold in small local regions around each cell. The result of the traversability analysis is a classification of unknown (unobserved height), traversable, or fatal, along with the classification of observed or virtual provided with the height map.

The main planner utilized is hybrid A*, as detailed in [10]. Planning is conducted on a graph where nodes are positioned on a 3-D grid with the same 0.1 m spacing utilized in the height map, and 30° in yaw. Edges are derived from motion primitives and cost dynamically as they are visited by A*. Costs were tuned to provide the desired balance between longer paths with gentler slopes and shorter paths with steeper slopes.

1) PATH FOLLOW

In order to improve robot navigation performance and efficiency, and prolong the lifespan of robot hardware, improvements to the velocity command generation were deemed necessary, leading to the development of a new trajectory generation behavior.

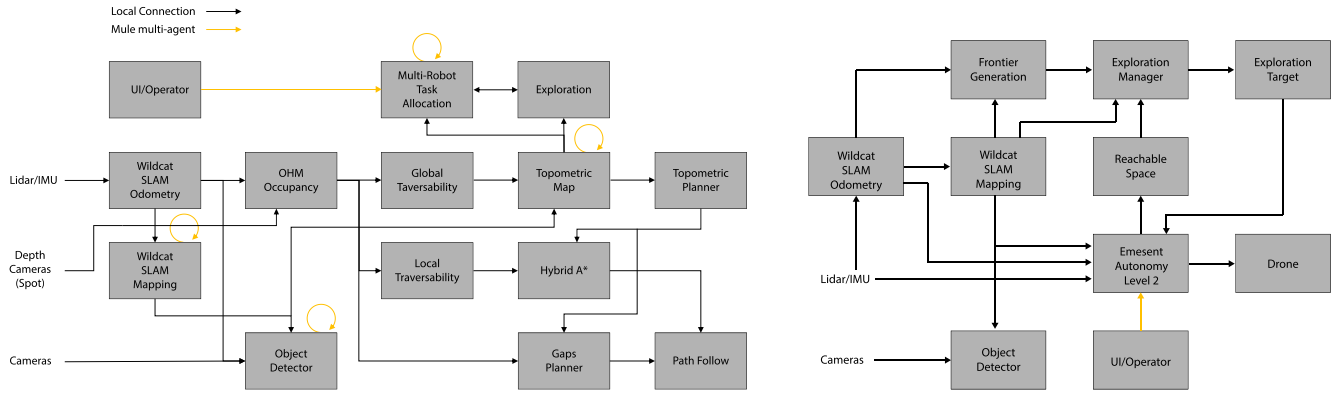


FIGURE 12. Block diagram of autonomy system, (left) for the UGV, and (right) for the UAV.

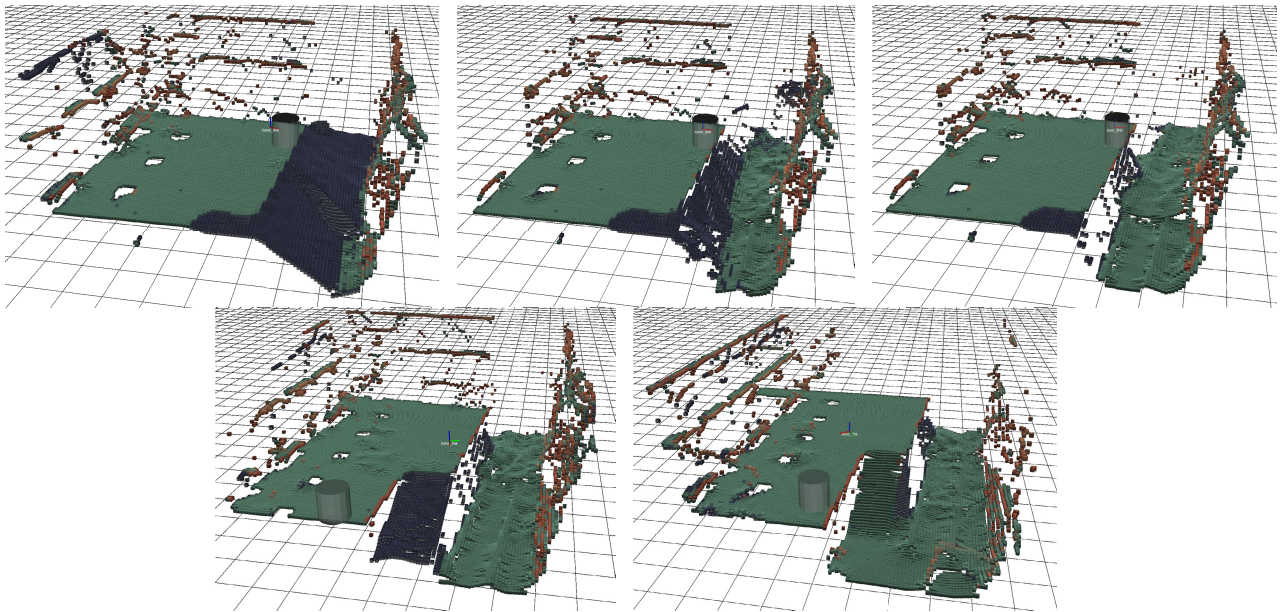


FIGURE 13. Virtual surface processing during final circuit event: (top left) a spot robot autonomously traverses the subway platform, showing a virtual surface falling off the edge of the platform down to the tunnel. (Top center) As the edge is approached, the virtual surface becomes steeper. (Top right) This progresses until the steepness reveals the fatal cost at the edge of the obstacle. (Bottom left) The robot moves toward the front part of the platform, identifying a virtual surface above the stairs leading to the base of the tunnel. (Bottom right) The stairs are observed, revealing traversable terrain leading to the tunnel base.

The new “Path Follow” behavior was developed with three key requirements in mind as follows.

- 1) Generated trajectories must strictly adhere to set velocity and acceleration limits.
- 2) Generated velocity commands must be continuous and smooth.
- 3) Overall performance must match or exceed previous systems.

The new Path Follow behavior meets these requirements through the use of actively updated tenth-order Bézier curves to generate trajectories from the robot base link to a local goal pose. Trajectory generation is optimized such that the form of the trajectory fits the input path as close as possible whilst also adhering to the kinematic

constraints of the robot and minimizing trajectory completion time.

The Path Follow behavior makes use of a dynamic short horizon envelope which reaches out from the base link of the robot platform out to the nearest obstacle, defined as at least one fatal cell in the cost map. The horizon defines the pose of the local goal, used as the target for all trajectory generation. The local goal is located on the local path at its intersection with the horizon. The horizon shrinks and grows as the robot moves closer to or further from obstacles and as it does, Path Follow dynamically adjusts the scaling of the robot’s kinematic limits thus slowing the robot as it approaches obstacles. This slowing around obstacles allows for more precise path tracking around obstacles, and is essential for narrow-gap navigation.

A key component of Path Follow is the generation of smooth and continuous trajectories and velocity commands. Newly generated trajectories are generated with specifically set control nodes such that the initial state of the trajectory matches the last robot command. This ensures a smooth continuous kinematic command profile sent to the robot platform whilst constantly regenerating trajectories, and is essential for accurate path tracking.

Active trajectory regeneration is attempted at a rate of 25 Hz. If a new active trajectory is generated, robot commands are set as $R = T(\Delta t)$, where R is the generated set of robot velocity commands in a twist format and T is the trajectory function with t time as input. If a new trajectory cannot be generated which fits current kinematic constraints the existing active trajectory is iterated and robot commands are set as $R = T(t + \Delta t)$. In the rare occurrence that trajectory regeneration fails continuously and a full trajectory is executed, a safety mechanism is built into every generated trajectory to ensure a safe stopping procedure is commanded at the end of each trajectory.

Path Follow works in conjunction with the rest of the behavior stack and as such has been tuned to be quite aggressive. Path Follow will attempt to follow any given path as best it can regardless of whether the route of the path may result in collision with obstacles. Instead, Path Follow will merely slow the robot down to a minimum speed, continue to follow the path, and rely on other recovery behaviors such as the decollide and orientation correction behaviors to recover the robot from any potentially dangerous collision state (described under other behaviors below).

2) GAPS PLANNER

The 0.1 m discretization resolution utilized in the hybrid A* planner is a significant limitation when seeking to pass through 800 mm doors with an ATR that is 780 mm wide.⁶ The gaps planner was developed to handle this type of case.

Initially, the development focused on RL approaches. The method in [36] was successful 93% of the time in simulation, and 73% of the time in on-robot tests. Despite these promising results, in the context of SubT where the a priori unseen environment is a large part of the challenge, a conventional planning approach was preferred. The final course demonstrated the motivation for this decision: the course contained many tunnels that were far narrower than anticipated or previously encountered. The hand-engineered gaps planner adapted well to this type of environment, whereas the RL-based method that was not trained on data similar to this would not have been expected to generalize well.

The gaps planner can be seen as an extension of hybrid A*, which integrates a continuous optimization step into the search to allow fine repositioning of search nodes within their respective discretization cells. The search proceeds similar to regular A*, but when cells are visited, the optimization

⁶The smaller width of the Spot robots was such that difficulties were not encountered and this behavior was not required for that platform.

step seeks to improve the continuous position and yaw of the node based on the predecessor node and the nearby obstacles. Critically, this allows search nodes to be reliably found when passing through tunnels and doorways that were within one cell's dimensions of the vehicle size (as with hybrid A*, the position discretization was 0.1 m, and the yaw discretization was 30°).

In addition to the improved planner, it was also critical to raise the platform's capability to accurately execute the plans. The combination of the hardware upgrades described in Section II-A1 and the development in Section IV-A1 provided the required enhancement. Particularly important was Path Follow's adaptive speed control, which reduces velocity based on the distance to an obstacle, allowing for the most accurate control in critical circumstances.

3) OTHER BEHAVIORS

Specialized recovery behaviors were developed that have priority in scenarios that may place the robot in an unrecoverable state. The orientation correction behavior activates if the pitch or roll of the robot may lead to the agent tipping over. The Decollide behavior moves the robot to a nearby nonfatal region, recovering from the case where a fatal cost appears within the footprint of the first search node preventing a valid path from being generated.

For the urban circuit, a dedicated stair climb behavior was developed for the Superdroid tracked platforms. This behavior utilized the extension of the robot flipper arms to extend the functional base of the robot, lengthening the lever arm required to tip the agent and preventing toppling down the stairs during ascension or descent. This behavior could be manually activated by the operator or set to automatically activate when the agent orientation exceeds a pitch threshold. This allowed the operator to teleoperate the agent onto stairs at which point the behavior would take over and complete the rest of the traversal in a safe manner (demonstrated during the urban circuit). Work on autonomous stair detection was deprioritized along with the Superdroids after the addition of the Boston Dynamics Spot robots to the team. Not only were the Spot's much more agile over a wider range of terrain conditions, their ability to handle stairs was superior to the tracked platforms that are unable to perform complex maneuvers on stairs (for example, stopping and turning). Details on stair climbing with Spot are discussed in Section IV-A4.

4) SPOT INTEGRATION

The Spot platform was a late inclusion in the team, with integration work commencing in April 2021. The platform quickly evolved into a highly capable team member which provided unique capabilities traversing stairs and tight passages.

We found it critical to integrate Spot's internal cameras in order to address stairs and negative obstacles, since the location of our pack (see Fig. 2) provided limited visibility at steep elevation angles in front of the robot, and no visibility behind (note that the Spot robot must reverse down stairs

due to its leg design). Spot's internal navigation capabilities presented many choices for integration with the autonomy stack. Spot internally generates a high-resolution (0.03 m) height map to a range of 1.9 m based on its five depth cameras. Initially, this height map was blended with the lidar height map generated by OHM, and the plan produced by hybrid A* was truncated at the point where it departed the local map. However, this resulted in two problems, first relating to the plans themselves, and second relating to the quality of the height map.

The difficulty encountered with the first approach for path planning was that Spot's internal planner appeared to generate plans that approximated a slerp (spherical linear interpolation) of the current pose and the provided goal pose, rather than constructing plans that are logically consistent with the environment. This was acceptable in more open environments, but sometimes prevented navigation in narrow corridors. Consequently, the local plan produced by hybrid A* was passed to Spot as a timed trajectory; this improved performance significantly and the trajectory was generally well-followed.

The difficulty with the height map was found when developing the capability to autonomously navigate stairs. Specifically, the difficulty occurred when the Spot commenced from the top of a platform from which stairs descended, but was positioned such that the stairs were not visible, but part of the ground plane at the bottom of the stairs was visible. In this circumstance, rather than marking the unobserved region as unknown, the processing hallucinated the continuation of the ground plane up to the edge of the top platform, without stairs. This was indistinguishable from an instance where there was a genuine negative obstacle, and so would prevent the platform from moving toward the edge to look for stairs.

In contrast, the OHM-based virtual surface processing would continue to approach the edge until either the stairs become visible, or the free space observed implies a non-traversable slope. To exploit this capability with the Spot, the native depth cameras were integrated into OHM. The front-left, front-right, and rear cameras were integrated into OHM at 5 Hz; the lidar provided adequate visibility on the sides and the side cameras were not found to be required. Due to the focus on supplementing lidar coverage at close ranges, camera rays were truncated to 2 m, and the resolution was decimated to match the height map resolution at that range. Online processing of this data stream and generation of virtual surfaces was possible with the GPU-based OHM implementation on the Intel NUC's integrated graphics.

Spot provides gaits for walking, crawling, and stairs. The stair gait is documented as slowing speed and pitching the body to observe stairs; testing appeared to indicate that it also conditions the robot to expect flat foot holds. Difficulties with autonomous identification of stairs due to the poor visibility from common viewing angles led to an approach which utilized the walk gait exclusively. This was partly

motivated by testing which showed that stair traversal in the walk gait was generally acceptable, whereas traversal of slopes or rough terrain of similar pitch in the stair gait was usually catastrophic. Because the spot leg design necessitates backward descent of stairs, the path cost was tuned to penalize forward motion down greater than a given angle, resulting in the desired effect. As discussed in Section VII-C, this approach was successful, and stairs were autonomously ascended and descended by Spot robots out of communications range during the final event. It is possible that improved stability could be obtained by switching to the crawl gait on rough terrain; experimentation with this concept is the subject of future work.

Typical battery life for the Spot was 40–45 min, which is insufficient to last an entire run. For this reason, a “battery return” behavior was incorporated, which forced the robot to navigate back to the base area when the battery percentage hit a critical threshold.

B. UGV GLOBAL AUTONOMY

The role of the global navigation system is to build an expanding map of the traversable terrain observed by all UGV agents, allowing any agent to navigate to any point observed by itself or any other agent. This is made possible by the PGO-based SLAM system described in Section III-A. Separate traversability maps (submaps) are generated for each root node in the SLAM graph, and like the SLAM frames themselves, traversability submaps are shared between agents.

As described previously, global autonomy utilizes the same traversability analysis as local navigation, but with maps generated with a longer range and at a lower rate. Subsequent observations which fall within the time range of the same SLAM root node are merged into the same image representation. Data with mismatching heights are handled by incorporating additional layers in the submap. The maps incorporate data for observed traversable and lethal surfaces; virtual surfaces are not incorporated into the map. Height maps and cost maps are also shared between agents; the data rate involved with these representations was found to be an order of magnitude lower than the SLAM frames. Compact graph representations of submaps are obtained by applying superpixel methods to the images, incorporating channels for the fatal traversability signal and height. Connections between submaps and submap layers are identified by finding superpixels which overlap between them. Global path planning is conducted utilizing A* on the graph with nodes corresponding to superpixels. Edge costs are obtained through distances, with additional penalties based on slope and roughness (averaged over the superpixel for each node), which are designed to match the penalties used in local path planning.

Dynamic obstacles present a particular challenge as paths previously observed as traversable must be updated to reflect the path that has been closed. The local navigation stack was capable of traversing extremely difficult terrain, but this sometimes took several attempts. It was important for the

global map update process to be tuned accordingly. It was also made difficult because both local and global navigation were based on height maps, and thus were unable to distinguish between a changed environment and difference in observation perspective of the same, unchanged 3-D structure. For example, from one perspective, we may observe the underside of a ramp crossing to an upper level, and declare an obstacle only where the clearance becomes insufficient. From another perspective, we may observe the top of the ramp, continuing up to the next level.

Because of this difficulty, the approach operated directly on the global superpixel graph. Specifically, whenever navigation failures occurred (i.e., timeouts without significant progress toward the goal), the source and destination nodes locations in the global graph were stored, and edges between superpixels containing those two positions were subsequently suppressed. The exception to this was edges which had previously been traversed by an agent. Because the cost of falsely mistaking the path home was high (e.g., preventing robots from returning to synchronize data), rather than suppressing these edges altogether, instead a high traversal cost was applied to them. Accordingly, any path not utilizing that edge would be preferred. In the case where the edge is still utilized, traversal failures will trigger task failures as described in Section IV-C, which will in turn trigger the selection of exploration tasks that have the potential to discover the necessary alternative routes. Overall, this approach was effective, but could take some time to resolve the correct map.

Whereas UGV exploration in earlier stages of the program was based on the 3-D point cloud visibility work in [42], in finals we utilized traversability frontiers, exploring to the boundary between observed traversable and unknown space. Thus, frontiers were attached to superpixels which bordered unknown space, performing a natural clustering of frontier pixels. Again, due to the multiagent global navigation representation, a region will only be marked as a frontier if it has not been observed by any UGV.

Connections are only made between submaps that are within a local neighborhood in the SLAM graph. Accordingly, if a region is revisited but loop closure has not occurred, the previously visited area will be explored as if it is being observed for the first time. This is a desirable behavior, as this additional exploration provides the data required for loop closure to occur. The process could likely be made more rapid by explicitly reasoning over the exact data necessary for loop closure (e.g., active SLAM, [26], executing actions aimed at collecting the data necessary for loop closure to occur).

Conceptually, the UAV could contribute to the UGV maps in the same way, but this was not exploited since the UAV does not run the same occupancy mapping, height mapping, and traversability analysis pipeline, and the raw data is prohibitively large.

Part of the global navigation graph from the final prize run is shown in Fig. 14.

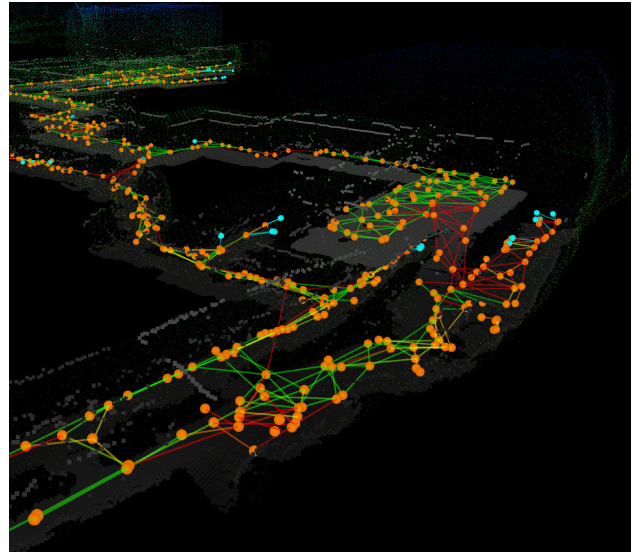


FIGURE 14. Portion of the topometric (global) graph constructed during the final prize run. The railway platform and stair portions correspond to the traversability maps illustrated in Fig. 13.

C. MULTIROBOT TASK ALLOCATION

The multirobot task allocation system provides the methodology for agents to autonomously and collaboratively agree on assignments of tasks to robots, based on a decentralized market-based process. This allows the collaborative assignment of tasks to continue as the communications topology changes. For example, if two robots are deep in the course and have communication with each other but not with the base station, they can seamlessly continue negotiating task assignments.

Each agent is allocated a bundle of tasks. The metric which task allocation seeks to optimize is the total reward of the bundles, where rewards have an exponential time discount based on the expected completion time of the task. For example, if we denote the bundle for agent a as $\mathbf{p}_a = (j_{a,1}, \dots, j_{a,n_a})$, the reward of task j as c_j , the traversal cost from task j' to j as $t(j', j)$, and the duration of task j as $T(j)$, then the total reward is

$$S(\mathbf{p}) = \sum_{a=1}^A \sum_{i=1}^{n_a} \lambda^{\tau^{a,i}(\mathbf{p}_a)} c_{j_{a,i}} \quad (1)$$

where

$$\tau^{a,i}(\mathbf{p}_a) = \sum_{k=1}^i t(j_{a,k-1}, j_{a,k}) + T(j_{a,k}) \quad (2)$$

where $\tau^{a,i}$ denotes the time when execution of the i th task $j_{a,i}$ completes, and $t(j_{a,0}, j_{a,1})$ denotes the cost of navigating from the agent's current position to the first task. The consensus-based bundle algorithm (CBBA) operates by building the bundle incrementally, bidding on the task which produces the largest increase in the bundle reward, where the

reward increase is evaluated by inserting the task into the best position in the bundle.

The primary task utilized by the task allocator is exploration. For the exploration task, frontier nodes identified by global navigation are clustered to provide tasks consisting of frontiers that are nearby in terms of global path distance. Each agent independently generates its own set of frontiers and tasks based on traversability data received from all agents. This avoids the solution of a decentralized clustering problem (which would be greatly complicated by regular periods of disrupted communication). Duplicate assignments are avoided by treating nearby tasks belonging to different agents as equivalent for the purposes of bidding, so that the assignment of an agent to a task requires outbidding another agent assigned to nearby tasks.

Tasks can be bid upon at any time, and new tasks continually arrive as agents move through the region. Each agent maintains its task bundle, which is limited to a maximum number of tasks, and a maximum expected duration. Because of the open-ended nature of exploration tasks, their duration is set such that two exploration tasks will not be added to the bundle at the same time. In order to allow the bundle to be adapted once it is full, we consider bidding actions which drop the final element from the bundle sequence and add a new element (into an optimized position, as is standard in the bidding process).

Methods were developed which estimated the reward of a frontier through bounds on the new volume that might be observed from the candidate pose. However, this was found to be counter-productive, since features such as narrow tunnels and tight doorways were of critical importance. Thus, without cognizance of this higher level semantic information, the standard reward estimates were found to be unhelpful, frequently triggering undesirable behavior (e.g., stopping exploration of a region of interest in favor of a more open area). For this reason, exploration tasks have a fixed reward, such that selection is based purely on the path cost.

Motivated by Brass et al. [4] and by the tree-like structure of many of the environments of interest, we encourage the agents to separate by penalizing the shared component of the path from each robot back to the base. In [22], this is shown to improve performance in environments that are well approximated as trees.

As well as exploration tasks, the task allocator also supports “return to synchronize” tasks (i.e., return toward the base until all data is uploaded to and downloaded from the base), and “drop node” tasks. Synchronization tasks benefit from multiagent implementation so that if another agent is in a location that allows it to return more quickly and it has all of the data from the agent that needs to synchronize, it can bid on the task. Drop node tasks are manually generated, and can be executed by any agent that has a communications node available. Logic was developed to automatically deploy communications nodes based on signal strength, but it was not deployed in competition due to the risk of rendering a

narrow tunnel impassable. Further details of the task allocation method can be found in [22].

D. UAV AUTONOMY

The UAV autonomy used in the final competition broadly follows the autonomy used in previous competitions, with improvements focused on exploration. The UAV utilizes the navigation functionality commercially offered by Emesent as Autonomy Level 2, providing both local and global navigation solutions.⁷ The UAV features a manager node to coordinate local and global planning, and implement core behavioral primitives. The manager receives higher level tasks from the operator, such as move to these waypoints and explore. It coordinates activities to achieve these tasks, and interfaces with the lower level autonomy. This modular architecture has simplified the process of continual improvement to our higher level autonomy functionality.

To ease operator load, the UAV supports four major control modes: exploration, 3-D waypoints, 2-D waypoints, and planar waypoints. Three-dimensional waypoints specify an exact position in space where the UAV must move, useful to get the UAV into narrow openings when other alternatives are available (i.e., moving into a shed). Two-dimensional waypoints specify a location in the horizontal plane, but leave height free, which is useful for general-purpose commands. Planar waypoints simply require that the UAV reach any point on a user-specified plane, but does not specify where. It is often selected as a vertical plane, in order to provide a direction of travel without the need for a precise goal. This is useful for sending the UAV to a general location (i.e., not just basic exploration) in a space whose approximate layout is very roughly known, e.g., go 100 m down a tunnel and then turn left at the branch. It can also serve as another form of more directed exploration.

Frontier generation and selection broadly follow that described in [42], with frontier selection based on a scoring function balancing frontier size, proximity, and alignment with previous exploration. Improvements focused on dealing with invalid waypoints, motivated by experiments at an indoor paintball course. The paintball course featured many small windows, narrow doorways, and other nontraversable apertures which generated a large number of frontiers that were not reachable by the UAV, causing exploration to become stuck for significant periods of time. Mitigation efforts focused on utilizing traversability information provided by the planner. The planner published its search tree after every planning iteration, which the exploration code used in two ways. The first was checking whether the planner was able to find a path sufficiently deep into a given frontier. If so, the frontier was marked as reachable, and its score for selection purposes was increased, strongly biasing exploration toward known-reachable frontiers. Furthermore, the closest point to the center of a reachable frontier was retained

⁷Emesent AL 2 (2021) <https://www.emesent.io/autonomy-level-2>.

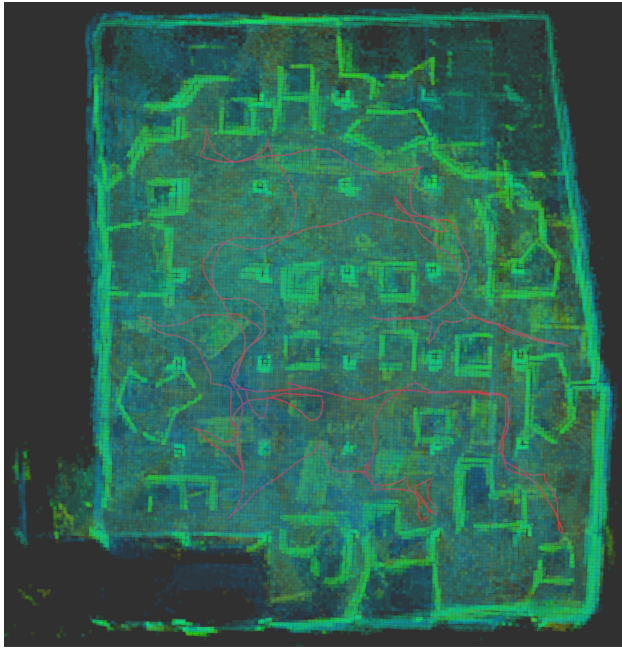


FIGURE 15. Trajectory of UAV (red line) performing exploration at an indoor paintball course prior to the final competition. The background color shows height, illustrating the UAV's path through the maze-like course.

as a witness point. When a frontier was cleared, other frontiers that contained the witness point of the cleared frontier would be marked as reachable. This provided additional robustness when frontiers were modified at distances that exceeded the planning horizon, which was particularly important for large open spaces. An example exploration trajectory of the indoor paintball course is shown in Fig. 15.

Previously, a frontier was only marked as unreachable if the UAV had failed to make substantial progress toward a frontier for 20 s. These delays caused by unreachable frontiers were reduced by identifying when the UAV was moving away from the target frontier, indicating that the frontier was unreachable. To do so, the exploration manager would compute the minimum distance from the search tree to the target frontier, and if below a threshold (3.2 m) indicating that the UAV was in close proximity to the target frontier, it would compare the search tree distance to the distance from the end of the actual plan associated with the search tree to the frontier. The path end distance being significantly larger than the search tree distance (2 m) indicated that the path directly to the frontier was blocked, and the planner was attempting to find an alternate route. In this case, the exploration manager would mark the frontier as unreachable, and exclude it, and any other frontiers with centers inside the unreachable frontier, from consideration.

The previous iterations of the UAV exploration code ignored the global structure of the environment, using only the direct Euclidean distance between UAV and frontier when selecting frontiers, with obvious downsides in larger or more

complex environments. For the final competition, the UAV exploration manager was enhanced to use the SLAM pose graph to reason about the global environment. When a frontier was created, it was associated with a frame in the pose graph, and the UAV was continuously associated with the currently active frame used by the SLAM module. Unfortunately, global SLAM optimization had significant latency, often exceeding 10 s, leading to poor associations. As a result, frontiers and the UAV were reassociated with the closest of their original frame and neighboring frames in the pose graph. When selecting a frontier, the UAV was limited to considering frontiers that were, after reassociation, associated with frames adjacent to the UAV's current frame in the pose graph. This limited consideration to frontiers that could be reasonably expected to be reachable by the local planner. If there were no frontiers in the adjacent frames, the UAV timed out in making progress toward a frontier, or the UAV marked its current frontier as unreachable, then the exploration manager would check if relocation was required. The relocation was required if there were no frontiers marked as reachable associated with the current UAV frame or adjacent frames. If relocation was required, the UAV chose the frame associated with the most, reachable frontiers, tie-breaking in favor of frames with more total associated frontiers. The exploration manager then used the SLAM pose graph to compute a path to the target frame, relocated there, and then restarted exploration.

V. PERCEPTION

The camera-based perception framework used in the final event was similar to that used in the earlier circuit events, wherein artifacts detected in the camera stream by the DeNet object detector [39], [40] were localized in 3-D using lidar depth measurements. Two major additions to the framework for the final event were the introduction of multiagent artifact tracking and sending updated information of a previously detected artifact.

The main purpose for the introduction of the multiagent artifact tracking was to reduce the number of artifact reports seen by the operator. For the urban circuit, each agent tracked artifact locations in the odometry coordinate system and thus any drift in the odometry trajectory could possibly result in new detections being erroneously associated with known artifacts. These errors were mitigated at the urban circuit by removing known artifacts from the tracker memory when they had not been detected for 30 s or the agent was more than 30 m away from the artifact. Unfortunately, this meant that an agent would redetect artifacts when visiting previously explored space. Maintaining the position of artifacts in the global map alleviates the issue of drift and thus artifacts can be remembered indefinitely. The similar problem of one or more agents visiting the same area and detecting the same artifacts can also be mitigated by using Wildcat's loop closure capability to establish correspondence between each agent's global map (see Section III-A for more details).

The need to update information of a previously detected artifact was to address a common problem when using the

artifact tracker to eliminate duplicate detections. In some instances, a true-positive would be correctly identified by the object detector but the operator was unable to confidently confirm the detection in the image because the artifact was either poorly illuminated or too small. For the final event, we introduced a policy where the operator GUI was updated with subsequent detections if the detection was at least 1 m closer than a previously sent detection. The operator could then scroll through all of the artifact observations in order to more confidently confirm the detection. This functionality was easily implemented by assigning every tracked artifact a globally unique identifier and including the identifier in every sent artifact report.

The training dataset continued to expand after the urban circuit. The dataset used to train the DeNet detector model for the final event consisted of over 30 000 images of the nine artifacts at 12 different locations (21 000 annotated and 9000 negatives). The images were captured using a variety of mobile phones as well as the cameras used by the UGVs and UAVs.

WiFi and gas detections were presented to the user as a marker located at the position of the respective agent when detection occurred, and colored by the strength of the detection (i.e., RSSI for WiFi, and detected density for gas). This provided the necessary information for the human supervisor to either detect and locate the respective artifact, or command a robot to collect additional information. As discussed in Section II-C5, the active scanning required for Bluetooth detection was found to cause significant communications disruption, so Bluetooth detection was disabled. Accordingly, we were reliant on WiFi detection for cell phone artifacts (a visual detector was trained, but in practice due to the small size and indistinct appearance, it was rarely detected), and visual detection for the cube artifact.

VI. HUMAN-ROBOT TEAMING

The role of the human supervisor was to provide high-level guidance to the robots while assessing incoming object detections and sending reports to the DARPA server. As the number of platforms increases, the bandwidth for a single human supervisor to manage individual agents becomes limited.

Previous experience showed the value of providing the human supervisor with a full control range of the robots. While the dominant mode of operation was autonomous, fallback modes including waypoint navigation (or, more generally, missions consisting of scripted sequences of operations) and teleoperation proved useful in unexpected situations. With the focus on autonomous operation, interfaces were provided to permit entry of high-level guidance, in the form of prioritization regions. These were specified geometrically, altering task priorities either within a region, or for any task downstream of the region in the shortest path tree commencing from the base location; examples of this are illustrated in Fig. 16. These latter graph-based priority regions were found to be a particularly valuable improvement, as they allowed

prioritization of a region of unknown shape and extent which lay beyond a junction.

A multimodal task-based graphical user interface (GUI) enabled the human supervisor to efficiently assess the status of each platform at a glance and provide mixed-level commands as needed (from teleoperation to fully autonomous exploration). Chen et al. [6] described details of the user interface employed at the final event.

The operator interface was separated into two distinct windows: an artifact review window for efficiently assessing RGB images from detected objects and their localization, and an operations window for interfacing with the robots. The example in Fig. 16 shows the operations window for interfacing with three robots in autonomous exploration, illustrating prioritization regions, and interactive task markers, which allow the operator to manually assign or cancel individual tasks. The human supervisor can assess several components of the robot's health by glancing at the colored octagonal ring around the robot markers, including the communication rate, percentage of data missing from the ground station, mission state, and any errors. The robot markers are a depiction of the robot type, and for the ATRs, display the number of remaining communications nodes and the UAV launch state.

The artifact review window presents the operator with both a list of objects and a map view showing their locations. The operator can quickly scan through new detections and either save or reject them. Gas and WiFi detections are illustrated by markers showing the detection location, with opacity indicating the concentration and signal strength, respectively. In this case, the operator infers and indicates the source location on the map.

VII. RESULTS AT THE FINAL CIRCUIT EVENT

The final event was held at the Louisville Mega Cavern in Kentucky, USA, on September 21–24, 2021, and consisted of two preliminary rounds (30-min runs conducted on September 21 and 22) and a final prize round (a 60-min run conducted on September 23). Team CSIRO Data61's objectives for the preliminary runs were to maximize information gained from the course and ensure each platform was fielded before the prize run while minimizing risk to hardware. Without a full set of either human or robot team members (due to COVID-19 travel restrictions), the robot roster for the three circuits faced in Louisville was carefully deliberated. Any postrun repairs could only be performed by a skeleton crew with over-the-shoulder support from experts in Australia using telepresence robots.

Based on extensive testing, the ATR robots (Rat and Bear) were trusted as exceptionally robust in a wide range of unstructured conditions, while the Spot platforms (Bluey and Bingo) had greater strengths in terrain coverage, and were particularly critical in urban areas (for example, with narrow stairs). The aerial vehicles (H1 and H2) were reserved for open locations in the course with high ceilings. These preconceptions guided strategic planning for the preliminary

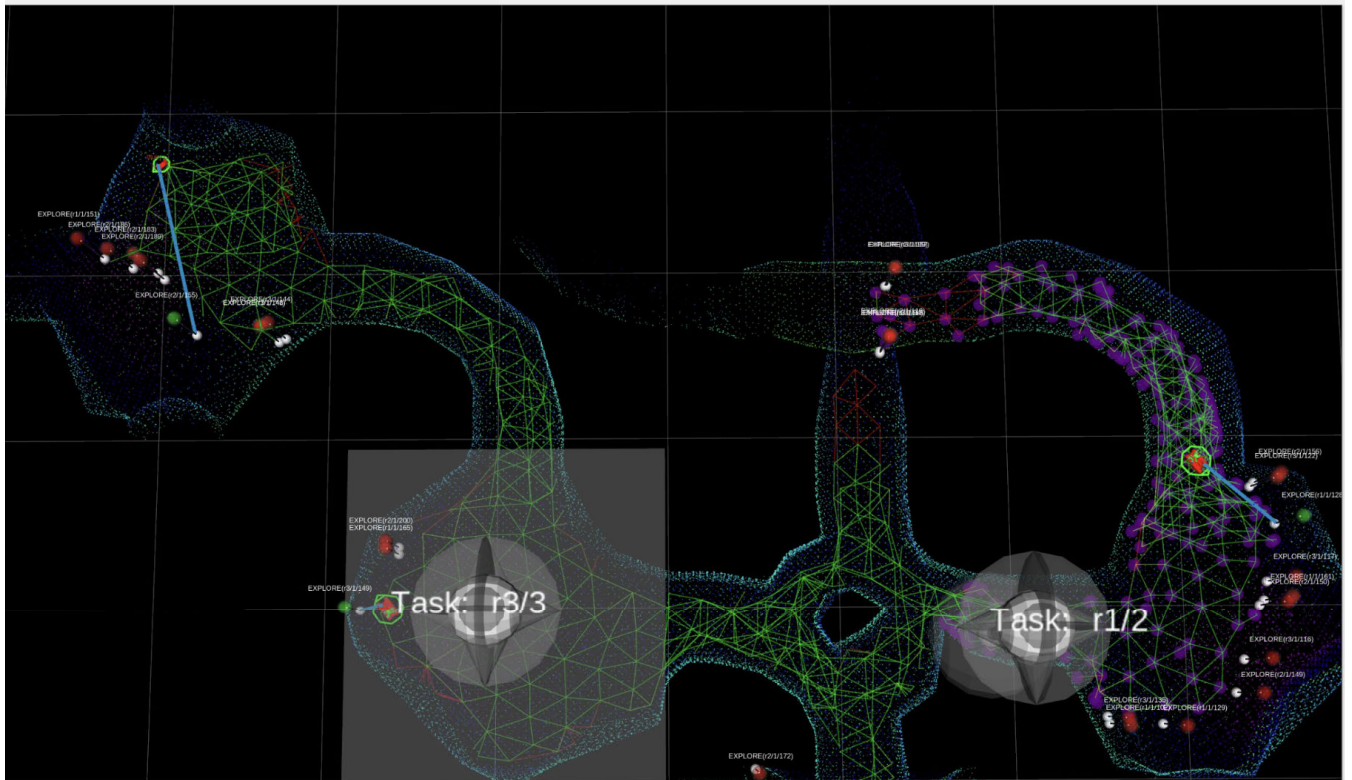


FIGURE 16. Example of the map-based GUI in the operations user interface. Interactive “lollipop” markers enable the operator to manually assign or cancel tasks. The box in the lower left of the image defines a geometric prioritization region “Task: r3/3” for robot r3, and “Task: r1/2” defines a graph-based priority region for robot r1 (where the affected part of the graph is shown with purple shading). The octagon indicator surrounding the robot shows various aspects of status including SLAM, navigation, communications, and tasking.



FIGURE 17. Aerial view of the shade-cloth tunnel with an overall length of over 300 m built at CSIRO’s QCAT site in Pullenvale, QLD, Australia (left), an inside view (center), and stairs and mezzanines built inside the tunnel (right).

runs. For each preliminary run, both ATRs would enter the course carrying deployable communications nodes, alongside a single Spot. For the first preliminary run a single UAV was carried by one of the ATRs, in the second preliminary run a UAV was attached to each ATR. This roster allowed for redundancy, in the event of misfortune with a Spot or UAV, there would be a set of platforms available for the final event.

The Spot robots were generally more agile over a wider range of terrain conditions than the large ATRs. The strategy

that evolved through testing was to send in a Spot robot first, followed by an ATR to bridge communications. Spot robots were able to autonomously traverse stairs, favoring urban settings, whereas the ATRs proved their robustness in challenging cave conditions. The confidence of the human supervisor in the abilities and limitations of each platform was cemented through extensive testing (based primarily on weekly test sessions at the CSIRO QCAT site, which incorporated urban industrial regions, a terrain park, and a synthetic tunnel environment shown in Fig. 17).

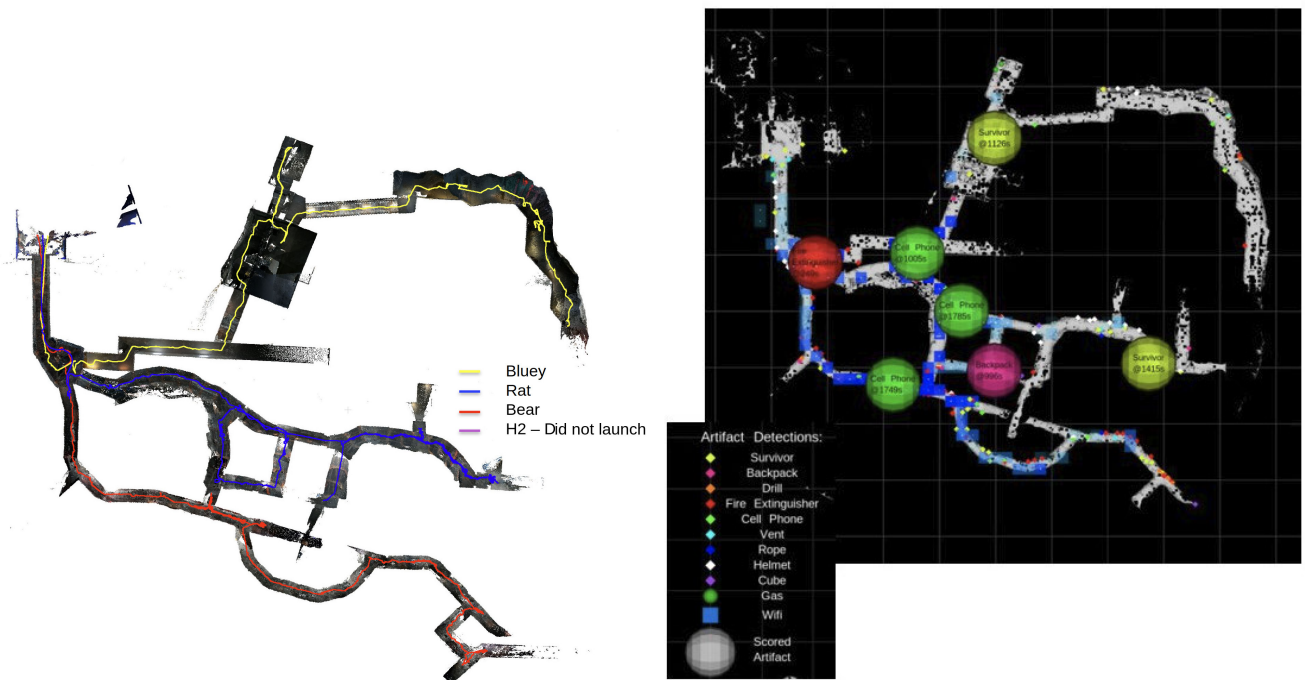


FIGURE 18. Course coverage and successful object reports for preliminary run 1. The starting area is located at the top left of each image. (Left) Robot paths by color for Spot robot Bluey, ATRs Rat and Bear, and UAVs H2 (which was not launched). (Right) The final map and object reports are based on information from the base station. The various artifact detections are shown as small dots in corresponding colors, while successfully scored artifacts are shown as large spheres, marked with the artifact time and scoring time (in seconds).

A. PRELIMINARY RUN 1

The agents sent into the first preliminary run were Rat (ATR) with marsupial UAV platform H2, Bear (ATR), and Bluey (Spot). Bluey was the first robot sent into the course, and upon confirming three distinct environment types (urban, tunnel, and cave, see Fig. 9), the supervisor elected to send Bluey to explore the urban section. Rat was sent into the tunnel environment, and Bear into the cave section. Fig. 18 shows the course traversal from each robot [see Fig. 18(a)], and the object class and location of reports that were correct [see Fig. 18(b)].

Communication nodes were placed at the entrance to the three sections, however, Bluey quickly lost communication with the ground station exploring the urban section. The connection was maintained between the ground station and the ATRs throughout the run. A connection was established between Rat and Bluey late in the run, enabling map information to be regained on the ground station. The recovered information revealed that Bluey had fallen while traversing train tracks in the urban environment (within the first 10 min of the run).

A total of seven objects were correctly detected and reported in the 30-min run; five were detected visually and two were WiFi detections of cellphones. Another three were successfully detected, however, did not make their way back to the ground station, or were not efficiently displayed to the human supervisor before the end of the run. One artifact was

detected but not reported as its probability was below the threshold for reporting. Postrun analysis revealed a fault on the 2.4-GHz channel of one of the communication nodes at the ground station, this was replaced before preliminary run 2.

The UGVs attempted to send a total of 188 visual artifact reports to the operator (6.26 reports per minute from all UGVs). Postanalysis of the sent reports showed that 13 reports were true positives and the remaining 175 were false positives. Approximately one-quarter of the false positives were due to artifacts being detected on the robot itself. This image mask configuration error was easily corrected in time for the second preliminary run.

Fig. 18 highlights that two or more robots explored the area near the start of the course as well as a passage which connects the cave and tunnel circuits. Analysis of the new artifact-sharing capability of the artifact tracker showed that 13 artifacts (true and false positives) were detected by more than one robot. This feature reduced the number of artifact reports sent to the operator for inspection by 17 reports.

B. PRELIMINARY RUN 2

The agents sent into the second preliminary run were Rat and Bear (ATR) both with marsupial UAVs (H1 and H2), and Bingo (Spot). Bingo entered first, and was sent into the urban environment. The human supervisor was unable to prevent Bingo from following the fate of Bluey from the first run. The robot quickly lost communication with the ground station,

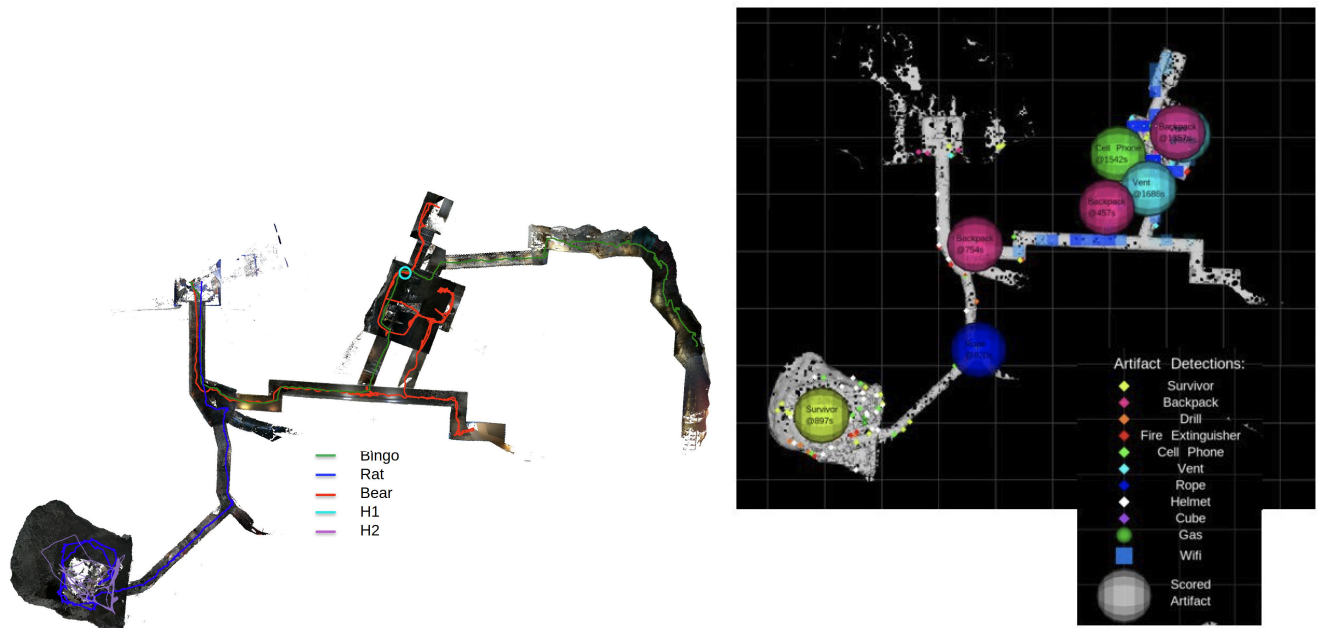


FIGURE 19. Course coverage and successful object reports for preliminary run 2. The starting area is located at the top left of each image. (Left) Robot paths by color for Spot robot Bingo, ATRs Rat and Bear, and UAVs H1 and H2. (Right) The final map and object reports are based on information from the base station. The various artifact detections are shown as small dots in corresponding colors, while successfully scored artifacts are shown as large spheres, marked with the artifact time and scoring time (in seconds).

and slipped on the train tracks early in the run (~8 min). Data from this robot was not recovered during the run.

Rat was tasked to operate in the cave environment and a small cavern was identified for launching a UAV. The UAV (H2) was launched successfully and thoroughly explored the cavern. Rat became immobilized soon after launch with a suspected motor fault and remained in the cavern for the remainder of the run.

Bear was sent after Bingo into the urban section attempting to improve the communications backbone, however, a dynamic obstacle had activated as Bingo entered a warehouse area preventing Bear from pursuing Bingo directly. A communications node was dropped with Bear at a junction expected to help with communications to Bingo, but this was not successful.

Bear explored several small office rooms before discovering an alternative entrance to the warehouse area. A second UAV (H1) was successfully launched in this area, however, the robot crashed spectacularly after ingesting debris soon after launch. Bear was the last active robot, and the final minutes were spent attempting to recover data from the lost Spot through the tunnel environment as in the previous run. Time ran out before this was achieved.

A total of eight artifacts were successfully reported during the 30 min run. Seven of the artifact detections were from visual detections and the remaining artifact was detected using WiFi. Importantly, we detected every artifact we observed. The UGVs sent a total of 106 reports for the run (average of 3.53 reports per minute). Postanalysis of the sent reports showed that 11 were true positives and the remaining

95 were false positives. Sharing artifact reports with all agents reduced the number of artifact reports sent to the operator for inspection by five reports.

Fig. 19 shows the course traversal and correct object reports from the second preliminary run. Fig. 20 shows examples of object detections from the UAVs. After the run, several repairs were conducted including replacing an ATR motor and fixing antennas on damaged communication nodes. Repairs were performed with long-distance support from Australia through “Double 3” telepresence robots from double robotics.

C. FINAL PRIZE RUN

All available robots were taken into the final prize run, including two ATRs (Rat and Bear), two Spot robots (Bluey and Bingo), and two UAVs (H1 and H2). Both Spot robots were sent in first, one into the urban environment (Bluey), and one into the cave environment (Bingo). Both ATRs placed communication nodes at the intersection of the three environments, then Rat was sent into the tunnel section, and Bear into the cave.

Bingo rapidly progressed through the cave environment, and quickly disappeared from communications. The human supervisor carefully de-prioritized the region leading to the train tracks in the urban section, preventing Bluey from repeating the mistake of the two preliminary runs. Bluey lost communications as it headed toward the train platform at the end of the urban section.

Rat explored the tunnel section, making slow progress over a tangled fire hose. The robot dropped a communications



FIGURE 20. Example object detections from the UAVs.

node at a junction, and made an unsafe turn over the rail of a mine track resulting in the de-tracking and immobilization of the robot (~28 min into the run). The tunnel was narrow and the ceiling height was too low to launch the UAV without risking catastrophic failure of the map. Bear made slow progress through the cave environment, successfully detecting an object in the small cavern (previously explored in preliminary run 2), then returning to the main channel of the cave to follow Bingo's path.

Approximately 30 min into the run, communications with Bluey were reestablished. While out of communications, Bluey had climbed stairs to reach the subway platform, explored the top of the platform, descended stairs to the subway tunnel, and exited toward the tunnel course. In the process, Bluey briefly reconnected with Bingo, and was subsequently able to mule part of its data back to the ground station. Bingo had located a large cavern at the end of the cave section, and had appeared to have fallen (post-run analysis confirmed Bingo fell at 22 min). The human supervisor directed Bluey toward the large cavern, and prioritized getting Bear to this location with a UAV.

Bear was unable to make progress through the cave environment with the UAV mounted on the back due to the low clearance of the tunnel. There appeared to be a path leading to the large cavern through the tunnel section, and the human supervisor directed Bear to backtrack to this location. However, a dynamic obstacle had closed the passage behind Rat, and the only alternative route was blocked by Rat, which was immobile. The human supervisor had to remove the UAV to enable the traversal of the narrow cave to recover data from the Spots. With time running out, the human supervisor relied heavily on teleoperation for faster traversal, ensuring communications were maintained (by dropping communication nodes along the way). Bear was controlled to the smaller cavern to launch the UAV, then made quick progress through the cave section toward the large cavern. In the final minutes, Bear established a connection with Bluey (fallen at ~40 min), and the final scored object detection came through to the ground station (reported at 25 s remaining).

A total of 23 objects were successfully detected. Another four objects were detected but not reported. Of these, one detection did not make it back to the ground station in time, and three nonvisual detections (gas and two cellphones) were difficult to localize given the high load of the human supervisor at the end of the run (see Table 3). Fig. 21 shows the course traversal for each ground platform and the scored object reports. Table 4 shows the percentage of object reports by platform type (ATR, Spot, and UAV). These results indicate the Spot robots were slightly better at detecting objects than the ATR's (more detections for each meter of terrain covered). This can be explained by the increased FOV from an elevated perception pack and reduced occlusion compared with the UAV-carrying ATRs. The UAVs successfully detected objects in the preliminary runs but were not utilized for object detections in the final prize run, as the ideal launch locations were not able to be reached by the UAV-carrying ATRs. The UAV that was launched in the prize run did not move from its hover position and did not report any detections; as previously described, it was launched in an already-explored cavern for the purpose of providing additional clearance for the ATR.

The mode of operation of each robot as a function of time is shown in Fig. 22, illustrating the use of the directed autonomy functionality to achieve the results previously described. A common pattern is the use of waypoints to position a robot in the desired area, followed by autonomous operation, either in the default mode (without prioritization), or using prioritization to ensure continued progress in the desired direction. For example, Bingo (r5) shows extensive use of prioritization regions to achieve the desired result, while Bluey (r2) shows both task prioritization regions and manual task assignment to direct it to the region of interest. Once Bear (r3) was the only functional agent within communications range, it was controlled using waypoints and later, in the time-critical period, using teleoperation. The percentage of a robot's run under each mode of operation is provided in Table 5, showing the degree of operator intervention for each agent as a percentage of the robot's total operational time.

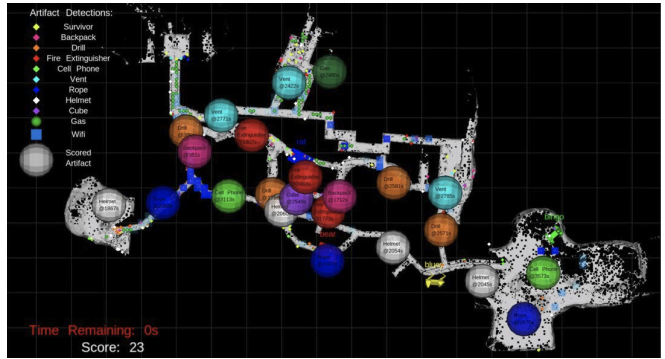
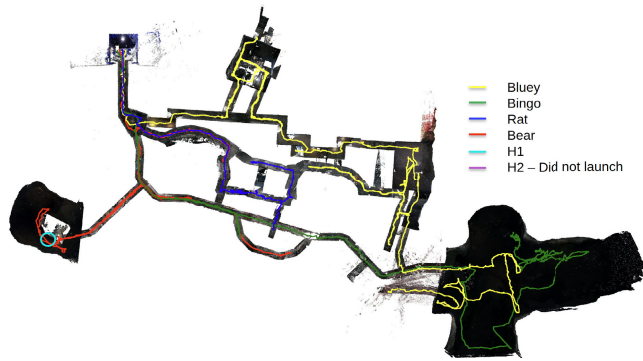


FIGURE 21. Course coverage and successful object reports for the final prize run. The starting area is located at the top left of each image. (Left) Robot paths by color for Spot robots Bluey and Bingo, ATRs Rat and Bear, and UAVs H1 and H2 (the latter of which was not launched). (Right) The final map and object reports are based on information from the base station. The various artifact detections are shown as small dots in corresponding colors, while successfully scored artifacts are shown as large spheres, marked with the artifact time and scoring time (in seconds).

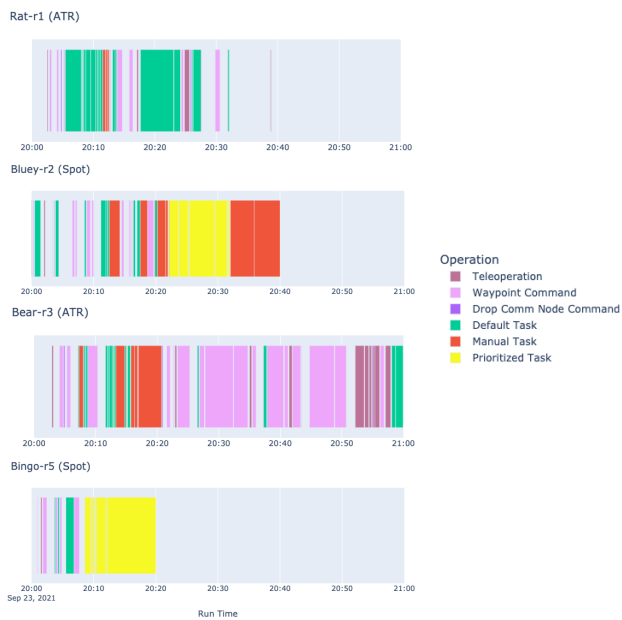


FIGURE 22. Mode of operation of the autonomy system by time for each UGV during the prize run. Teleoperation denotes direct joystick control, whereas waypoint command denotes navigation to a specified waypoint. Drop comm node command denotes an operator command to navigate to a specified location and drop a communications node. Default task denotes the regular autonomous mode of task allocation (without prioritization), whereas manual task denotes an operator override to execute a specific task, and prioritized task denotes task allocation where the selected task was in a region that had been prioritized by the operator.

The distribution of time that the ATRs spent using each planner, i.e., default hybrid A*, or the gaps planner of Section IV-A2, is shown in Table 6. The Spot robots are not shown as they only use hybrid A* (with the smaller agent dimension, the gaps planner was not found to be necessary). The table shows that the ATRs utilized the gaps planner for 21.3% of the time, or 22.9% of the time where a plan was active. This was much larger than expected, and is due

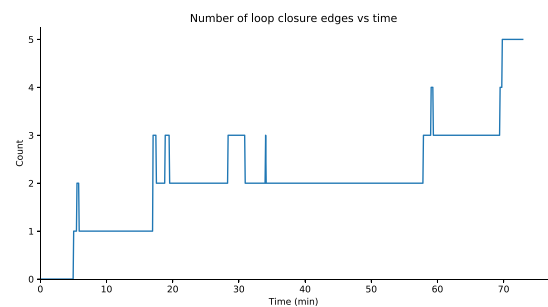


FIGURE 23. Number of loop closure edges (i.e., edges not implied by odometry) as a function of time during the final prize run. Note that the run ends at 60 min; loop closures after that point are due to the additional data subsequently relayed.

to the extensive narrow tunnels in the course. In most test environments, the gaps planner only activated in order to pass through narrow doorways; in this course, it enabled (slow) progress across parts of the course that would have been otherwise impassible.

The distribution of time that the robots spent using each behavior is shown in Table 7, focusing on autonomous motion-based behaviors, i.e., excluding teleoperation and stopped behaviors. As expected, the decollide behavior is utilized for a small proportion of the time, though its use reenables the path planning behavior. Orientation correction exists to prevent robot tipping, and saw a single activation for a fraction of a second.

The final pose graph for one agent (Bluey-r2) is shown in Fig. 11. The total number of loop closure edges in this graph is three. Fig. 23 shows the number of loop closure edges in the pose graph as a function of time (i.e., the number of edges that are not implied by odometry). When a loop closure occurs, there are often additional transient edges, which subsequently disappear as the graph is simplified, demoting some of the root nodes to become child nodes. The figure also shows that additional loop closures occurred after the end of the run (i.e., after the 60-min mark); these occurred as data from Bear (r3)


FIGURE 24. Example object detections from the UGVs.

TABLE 3. Summary of detection results in final prize run. *Cube counted as a visual, cell phone as nonvisual. †Data not communicated to base in time. ‡Nonvisual detection but too sparse/nonspecific.

	Visual	Non-visual*
Detected and scored	20	3
Detected but not reported/scored	1†	4‡
Passed but not detected	3	0
Did not pass	9	0

TABLE 4. Percentage of object detections and terrain coverage by robot type in the final prize run.

	Total Reports	True Positive	Terrain Coverage
ATR	43%	44%	49%
Spot	57%	55%	51%
UAV	0%	0%	0%

continued to be relayed through a slow (due to low SNR) communications link.

The agents sent a total of 203 artifact reports to the operator during the 1-h mission (an average of 3.38 reports per minute). Of the 203 reports, 29 reports were of true positives and the remaining 174 were false positives. An analysis of the new multiagent artifact tracking system showed that multiple agents had detected the same artifact (true positive or false positive) at 16 different locations and had reduced the number of duplicate artifact observations seen by the operator by

TABLE 5. Percentage of the prize run in each mode of operation for each platform, summarizing data in Fig. 22. See Fig. 22 for description of robot modes.

	Rat-r1 (ATR)	Bear-r3 (ATR)	Bluey-r2 (Spot)	Bingo-r5 (Spot)
Waypoint Command	15.8%	54.1%	11.5%	15.3%
Drop Comm Node	1.7%	1.3%	0.0%	0.0%
Teleoperation	12.5%	16.7%	1.6%	1.3%
Prioritised Task	0.0%	0.2%	31.3%	72.9%
Manual Task	4.1%	15.2%	41.5%	0.0%
Default Task	65.9%	12.5%	14.1%	10.5%

27 reports. Fig. 24 shows examples of object detections from the UGVs.

Fig. 25 shows the cumulative data generated by each of the autonomy processes of each ground agent during the final prize run. The figure shows that by far the largest contributor is the SLAM odometry frames required to permit each agent to build a unified map. Cost map bundles are the second contributor, which allows the building of the unified traversability map on top of the SLAM solution. Object detections utilize a similar amount of data, enabled by the tracking methods described in Section V. Task definitions and bundles and sync auctions represent data used by the task allocator to achieve a common understanding of the task set and robot-task assignments. Note that Bingo (r5) fell at around 20 min, but due to its resting position, odometry frames did not appear sufficiently similar to be suppressed, and thus the agent

TABLE 6. Percentage of the prize run where ATR robots utilized each planner (out of time when path follow behavior was active). “None” indicates that no planner was active, i.e., either the planner(s) are still generating a plan, or that no feasible plan was found.

	Rat-r1 (ATR)	Bear-r3 (ATR)	Overall ATR
Hybrid A*	78.0%	68.2%	71.6%
Gaps	15.1%	24.6%	21.3%
None	6.9%	7.2%	7.1%

TABLE 7. Percentage of the prize run where ATR robots utilized behaviors orientation correction, path follow, and decollide (focusing on autonomous motion behaviors, excluding stopped and teleoperation-related behaviors). *Path following is achieved through different behaviors on ATR and Spot, utilizing the method in Section IV-A1 for ATR, Section IV-A4 for Spot.

	Rat-r1 (ATR)	Bear-r3 (ATR)	Bluey-r2 (Spot)	Bingo-r5 (Spot)	Overall
Orient corr.	0%	0.002%	0%	0%	0.0008%
Path follow*	96.0%	93.3%	98.2%	97.4%	95.7%
Decollide	4.0%	6.7%	1.8%	2.6%	4.3%

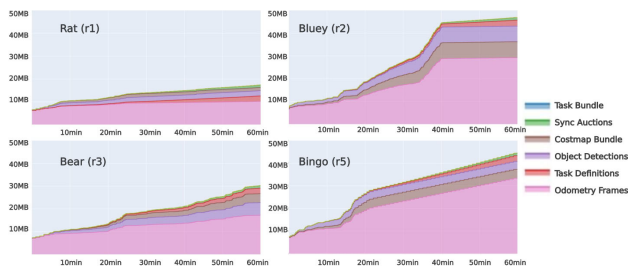


FIGURE 25. Cumulative data load (megabytes) for each of the ground robots during the 60-min final prize run.

continued to generate significant odometry data. Conversely, Bluey (r5) fell at around 40 min, and generated little odometry data thereafter.

Table 8 shows the average CPU usage for each of the processes on the perception pack, while Table 9 shows the average CPU usage for processes on the autonomy computer. SLAM, image processing, and object detection use similar CPU resources, although the latter two also use GPU resources. The heaviest CPU usage on the autonomy computer is OHM, which utilizes the GPU for ray tracing, and the CPU for data preprocessing and height map generation. Differences between ATRs and Spots are caused by the Spot’s different set of behaviors (e.g., passing a trajectory for a spot to follow rather than using path follow), higher speed, greater use of autonomous exploration (and hence task allocation), and processor differences.

As reported by Chung et al. [7], Team CSIRO Data61 excelled in the final prize run using alternate relevant

TABLE 8. Average percentage of CPU usage on the perception pack in the final prize run (where 100% denotes utilization of a full virtual core). Image processing encompasses image acquisition, rectification, and recording, and likewise, lidar/IMU encompasses the respective signal acquisition and recording.

	CPU usage (ATR)	CPU usage (Spot)
SLAM	136.5%	158.5%
Image processing	135.5%	140.5%
Object detection	127%	133.5%
Lidar/IMU	73%	72.5%
WiFi detection	13%	14%

TABLE 9. Average percentage of CPU usage on the autonomy computer in the final prize run (where 100% denotes utilization of a full virtual core).

	CPU usage (ATR)	CPU usage (Spot)
OHM (occupancy mapping)	117.0%	112.4%
Cost map generation	24.3%	27.2%
Behaviours	14.4%	7.4%
Hybrid A* planner	6.2%	12.6%
Gaps planner	22.0%	NA
Global mapping and planning	26.3%	29.0%
Exploration	6.0%	14.9%
Task allocation	5.1%	10.8%
Communications	2.0%	1.8%
External interfaces	40.5%	64.0%
Recording	47.4%	20.2%

evaluation metrics, achieving the lowest map deviation, greatest map coverage, highest report success rate (scored/submitted), and most accurate report with the smallest detection error (meters from ground truth). We were also the fastest team to enter the course with a robot (seconds from run start).

VIII. LESSONS LEARNED

The intensive development of the SubT program has provided us with a number of useful insights about how to conduct an activity of such scale. Some of these reflect things that our team did well, while others are hard-learned lessons where in hindsight we see the need to do things differently. In this section, we aim to chronicle some of these.

A. DEVELOPMENT AND TESTING

Prior to the tunnel circuit, a synthetic tunnel environment was constructed on-site, as illustrated in Fig. 17. Over time, this was expanded to include stairs, mezzanines, and a terrain park. Testing initially focused on this environment, but grew to incorporate as many elements as we could recreate on-site, for example, incorporating a long traverse from the tunnel to industrial warehouse regions. In the end, the team’s strengths and weaknesses reflect the environments to which we had regular access. We did not have regular access to

a representative underground communication environment, which made the development of features such as autonomous communications node dropping difficult to validate (thus this task remained manual).

Throughout the program, we maintained a regular cadence with weekly integration testing. These test activities served several functions; providing the team with a holistic view of where each person's work fits into the capability as a whole, enabling clear prioritization of work by regularly demonstrating the significance of different issues, and quickly revealing problems that arise when integrating work from multiple developers. While this process was invaluable in the lead-up to challenge events, during other development periods, some team members found it limiting due to the time occupied by the test itself, as well as the posttest analysis of results. Subsequently, in follow-on work, we have dropped back to fortnightly tests.

The weekly test regime greatly clarified the robustness requirements for agents. Platforms were run for many hundreds of hours, and the need to address issues arising from intermittent failures was highlighted by the impact they had on the overall test conduct and consequent team efficiency.

The team benefited from high standards in software development, including the use of continuous integration servers, and peer review through enforced pull requests. The high-quality Gazebo-based simulation environment was critical to development, and productivity was noticeably slower on features that were not adequately modeled in simulation but rather required extensive on-robot testing.

Due to the aggressive development schedule, it was regularly the case that hardware was not complete on the full robot fleet until shortly before each event. This last-minute scale-up of the robot fleet led to a range of issues. Again, this can be viewed as being related to limitations in simulation. For example, communications were not well-modeled in simulation, so extensive difficulties were experienced when the fleet was scaled up toward the end of the campaign, providing higher traffic and more complications unique to each platform class. Similarly, computational limitations of the simulation environment, in general, did not support testing of the full fleet size on available hardware; work has since been conducted to enable the use of parallel computing environments in simulation, permitting greater scaling.

B. PLATFORMS

Reflecting on the progression of our team's platforms, a key strength of our approach was a willingness to pivot rapidly, embracing opportunities to leverage developments in commercial offerings. Our original concept of operations centered around a bespoke hexapod design [33], with the goal of providing the ability to navigate extreme terrain. This concept was adapted based on two major learnings. First, the surprising capability of the tracked BIA5 OzBot ATR platform on rough terrain (e.g., slopes up to 60°) significantly changed our view of the tradeoff between platform types. Second,

the engineering effort involved in developing a platform to the point where it has sufficient robustness to be a viable candidate in the challenge context was difficult to sustain under resource constraints. As new, commercially available platforms emerged with the benefit of far greater engineering investments, the cost/benefit of bespoke development became less compelling.

Another aspect of our team's experience with platforms was the significant engineering effort required to adapt commercial platforms intended for teleoperation to robust autonomous operation. As described in Section II-A1, autonomous systems sometimes exerted control outside the designers' expectations, which led to outcomes such as motor burnout, and additionally, stock control systems made precise motion difficult. This was experienced with a range of wheeled and tracked platforms.

Throughout the duration of the program, the capability of commercial quadruped platforms has also increased greatly. As discussed above, our initial concept was on hexapod platforms based on the intuition that the additional legs would provide valuable improvements to stability on rough terrain. Again, the tremendous commercial investment in platforms such as Boston Dynamics Spot and ANYbotics ANYmal shows that the additional maturity of these quadruped platforms overcomes any advantage that an early prototype hexapod may hold. While these have come a long way, our own experience with Spot shows that falls on rough terrain is still an issue, and our original hypothesis regarding hexapod platforms may still stand, though the engineering investment necessary to test it would be large.

Finally, our approach of a common sensing pack and navigation stack paid large dividends throughout the program. All ground platforms utilized the same sensing solution and autonomy varied only through minor configuration parameter changes, and utilizing outputs at different levels (e.g., sending trajectories to Spot versus low-level control of tracked platforms).

C. SLAM

Our SLAM solution evolved significantly during the course of the program, especially in aspects relating to multiagent systems. Our solution was quite sufficient in the environments tested, and rarely presented a limitation to overall performance. However, there are a variety of qualifications for that outcome as follows.

- 1) The sensor payload with the spinning lidar is both expensive and heavy. In many applications, it is desirable or essential to use smaller, lighter, and cheaper sensor configurations. Understanding whether these sensor configurations can provide similarly adequate performance is a topic of further study.
- 2) SLAM performance appeared sufficient in the dust and smoke (e.g., fog machine) obscurants tested in SubT. This is specific to the obscurants encountered; each obscurant may react differently with the lidar signals.

- 3) Issues with place recognition for robot wake-up were addressed procedurally, in accordance with the competition rules. Robust and reliable wake-up location in more general problems remains a topic of interest.
- 4) Due to the environment scale and excellent odometry performance, place recognition was not found to be necessary for loop closure. This problem is still open for larger scale (spatial or temporal) missions, or systems with poor odometry performance.
- 5) The regime of sharing frames between robots and solving the SLAM problem independently on each agent was shown to be highly effective, but there are limits to its scalability. True distributed computation that accommodates larger scale but maintains the ability to address problems with poor communication remains an interesting, open problem.

D. AUTONOMY

One key point of realization for our team occurred in our local cave circuit event in September 2020. As described in [10] and [13], the ATR robots covered extreme terrain exceptionally well. They rolled on a number of occasions, each of which was a subject of close investigation. Some were due to subsidence of the terrain under the robot, a difficult problem that was un-modeled in the terrain analysis approach. Some were identified as unexpected conditions in the behavior stack, which were easily addressed. Most, however, occurred under teleoperation when the operator intervened to force the robot to navigate to areas where autonomy was refusing to go. The conclusion from this point was that the local navigation capability was at the point where, subject to the situation awareness constraints and latency experienced by the operator, autonomous navigation performed better on this terrain than teleoperation.

The conclusion on global navigation was somewhat different. Although performance has steadily improved throughout the development, it remains the case that the global maps have imperfections that benefit considerably from operator input. Most difficult is the tradeoff between falsely clearing frontiers in narrow doorways and failing to correctly clear frontiers when visited, leading to revisits of the same space. This is exacerbated by the fact that it is often difficult to distinguish traversable and nontraversable openings without attempting them.

A related lesson was on the scoring used for selecting frontiers. As discussed in Section IV-B, it was found that size-based scoring as is common in next-best view planners, often led to undesirable behavior such as declining to enter a small opening. In the SubT context where such traversals are of prime importance, our conclusion was that, in the absence of semantic analysis covering cases such as doors, size-based scoring was unhelpful.

Finally, the human/robot interface concept has come on an interesting journey, starting from a highly manual waypoint-based interface in the tunnel circuit, to relying on fully autonomous explore without the option for human input

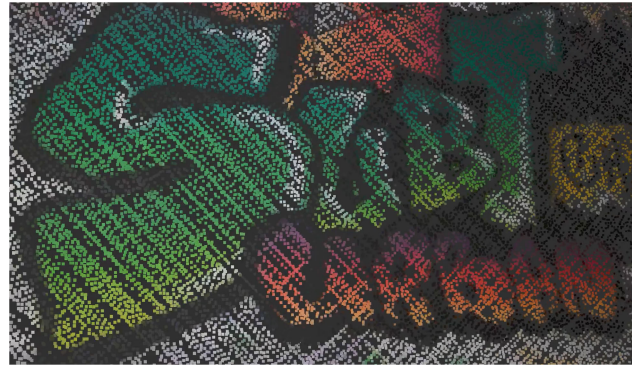


FIGURE 26. Raw colored point cloud showing a mural in the circuit, calculated online by Team CSIRO Data61's Blueey platform during the final event.

in the urban circuit, and finally arriving at a system which permits directed autonomy, with a complete set of tools for operator prioritization at the final event. The emphasis on the human/robot team in this concept significantly contributed to our result.

E. PERCEPTION

The object detection capability had interesting lessons related to the generalization error imposed by the competition structure. As much as we could collect test data in as wide a range of environments as possible, the unique and unpredictable nature of the environments presented in the challenge events inevitably led to significant model mismatch. Consequently, false detections were often a challenge, for which the only effective mitigation was temporal analysis (i.e., object tracking).

Another approach attempted but not deployed was to improve the operator's overall situational awareness via the use of a persistent colored point cloud. The goal was to augment the 3-D structure information computed by Wildcat from lidar data with color information obtained from each agent's onboard cameras. The displayed point cloud would dynamically update as the agents explored the unknown environment and would remain visible for the entire duration of the mission. It was hoped that the persistence would allow the operator to virtually teleport to any point in the explored environment in order to look for artifacts and/or make more informed decisions on each agent's progress or current task [41].

The feature was implemented to run in real-time on the agents with a resolution of one point per 30 mm³ voxel, and a rate of 4 Hz per camera, limiting bandwidth by compressing and sending only new points to the base station for visualization. The work required to reconstruct the point cloud on the base station was unable to be completed in time for the final event due to competing priorities.

A complete study of this functionality (including bandwidth impacts) will be pursued in the future; an example of the colored point cloud is shown in Fig. 26.

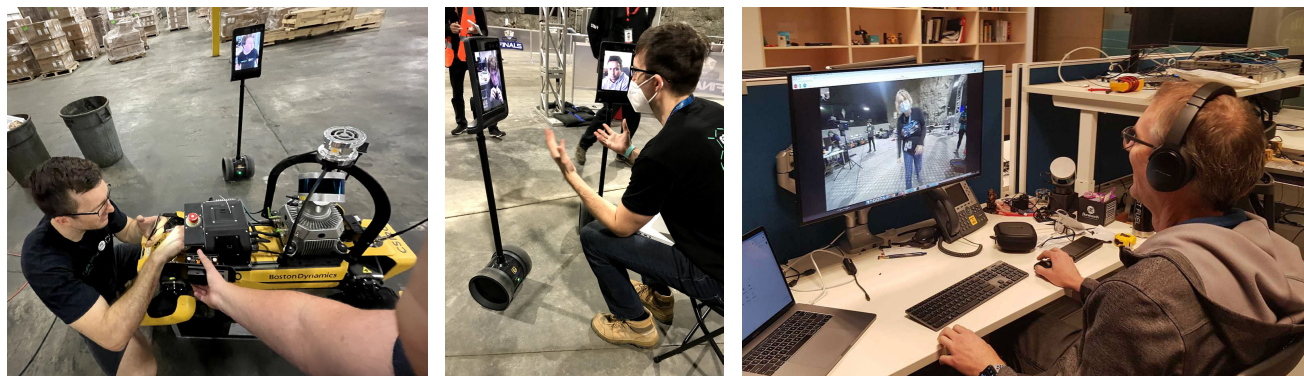


FIGURE 27. Engineer from the Australia-based team providing remote advice via telepresence robot to a U.S.-based team member to perform emergency electrical repairs on the Boston Dynamics Spot Quadraped's Autonomy payload (left), a U.S.-based team member providing run debrief to the Australia-based team after a preliminary run (center), and an engineer from the Australia-based team working U.S. East coast hours from Brisbane to provide support during the final event (right).

F. REMOTE SUPPORT

Finally, due to COVID-19 induced limitations on the composition of our deployed team for the final event led to a very challenging experience, where much of the development team provided remote support from the opposite side of the world. The Australian development team switched to the U.S. East coast time zone for the period of the deployment (i.e., both the lead-up and the actual event), and provided support through telepresence robots and video conferencing (see Fig. 27). Sending robot recordings back to Australia was challenging due to the lack of high-bandwidth connections in the deployed location, and was generally only achievable after stripping out all but the most critical data from the log files.

Hardware work performed by the deployed team included replacing an ATR motor, fixing wiring faults with an autonomy computer on a Spot robot, and replacing broken drop node compute modules. In each case, with the help of duplicate hardware held back in Australia, the development team performed the procedure, capturing detailed step-by-step instructions and photographs, which were sent to the deployed team who executed the procedure under remote supervision.

It was also necessary to be realistic about the robot team composition that could be supported. For example, a decision was made to not ship the DTR as it was not considered feasible for the small deployed team to support a fourth platform type.

IX. CONCLUSION

We have presented the system Team CSIRO Data61 deployed at the DARPA SubT Challenge finals. Special emphasis was given to the improvements and changes made to our systems and approach since Phase I (tunnel circuit) and Phase II (urban and cave circuits) of the challenge. The reasons for these changes were also explained. Results from the final event were presented and analyzed. We also provided insights and lessons learned over the overall campaign. The paradigm of using the same sensing and autonomy payloads on different

robot platforms allowed us to effectively scale our fleet. This also allowed us to pivot to new platform types with minimum lead time as demonstrated by us fully integrating the Spot platform into our fleet just a few months before the final event. In the final prize run, we had all but one of our robots being immobilized due to various challenge elements in the course leading up to the final minutes of the run. Despite this attrition of agents, the overall system performed as designed to provide resilience against this and we managed to create the most accurate maps of the environment as well as tie for the top score. Therefore, we have demonstrated how our paradigm of heterogeneous robot teams with unified perception and autonomy allowed Team CSIRO Data61 to achieve a remarkable outcome at the SubT Challenge finals, even without being able to send the full development team from Australia to the event in the U.S.

ACKNOWLEDGMENT

The authors would like to thank Nicolas Hudson, Erin McColl, Nicola Cowen, William Docherty, Megan Croker, Julie Noblitt, Dawn Lillington, Margaret Donoghue, and Alison Donnellan for their support leading up to and during the final event of the SubT Challenge. They also thank Tim Chung, Viktor Orekov, and the DARPA team for their extraordinary efforts and support during the SubT program.

The views, opinions, and/or findings expressed are those of the authors and should not be interpreted as representing the official views or policies of the Department of Defense or the U.S. Government.

REFERENCES

- [1] A. Agha et al., "NeBula: TEAM CoSTAR's robotic autonomy solution that won phase II of DARPA subterranean challenge," *Field Robot.*, vol. 2, pp. 1432–1506, Mar. 2022.
- [2] J. Bayer and J. Faigl, "On autonomous spatial exploration with small hexapod walking robot using tracking camera Intel RealSense T265," in *Proc. Eur. Conf. Mobile Robots (ECMR)*, Sep. 2019, pp. 1–6.
- [3] A. Bouman et al., "Autonomous spot: Long-range autonomous exploration of extreme environments with legged locomotion," in *Proc. IEEE/RSJ Int. Conf. Intell. Robots Syst. (IROS)*, Oct. 2020, pp. 2518–2525.

- [4] P. Brass, F. Cabrera-Mora, A. Gasparri, and J. Xiao, "Multirobot tree and graph exploration," *IEEE Trans. Robot.*, vol. 27, no. 4, pp. 707–717, Aug. 2011.
- [5] C. Cao, H. Zhu, H. Choset, and J. Zhang, "TARE: A hierarchical framework for efficiently exploring complex 3D environments," in *Proc. Robot. Sci. Syst.*, Jul. 2021, p. 2.
- [6] S. Chen et al., "Multi-modal user interface for multi-robot control in underground environments," in *Proc. IEEE/RSJ Int. Conf. Intell. Robots Syst. (IROS)*, Oct. 2022, pp. 9995–10002.
- [7] T. H. Chung, V. Orekhov, and A. Maio, "Into the robotic depths: Analysis and insights from the DARPA subterranean challenge," *Annu. Rev. Control, Robot., Auto. Syst.*, vol. 6, no. 1, pp. 477–502, May 2023.
- [8] T. Dang, M. Tranzatto, S. Khattak, F. Mascarich, K. Alexis, and M. Hutter, "Graph-based subterranean exploration path planning using aerial and legged robots," *J. Field Robot.*, vol. 37, no. 8, pp. 1363–1388, Dec. 2020.
- [9] K. Ebadi et al., "Present and future of SLAM in extreme environments: The DARPA SubT challenge," *IEEE Trans. Robot.*, vol. 40, pp. 936–959, 2024.
- [10] T. Hines et al., "Virtual surfaces and attitude aware planning and behaviours for negative obstacle navigation," *IEEE Robot. Autom. Lett.*, vol. 6, no. 2, pp. 4048–4055, Apr. 2021.
- [11] J.-T. Huang et al., "Cross-modal contrastive learning of representations for navigation using lightweight, low-cost millimeter wave radar for adverse environmental conditions," *IEEE Robot. Autom. Lett.*, vol. 6, no. 2, pp. 3333–3340, Apr. 2021.
- [12] Y.-W. Huang et al., "Duckiefloat: A collision-tolerant resource-constrained blimp for long-term autonomy in subterranean environments," 2019, *arXiv:1910.14275*.
- [13] N. Hudson et al., "Heterogeneous ground and air platforms, homogeneous sensing: Team CSIRO Data61's approach to the DARPA subterranean challenge," *Field Robot.*, vol. 2, no. 1, pp. 595–636, Mar. 2022.
- [14] J. Isaacs, K. Knoedler, A. Herdering, M. Beylik, and H. Quintero, "Teleoperation for urban search and rescue applications," *Field Robot.*, vol. 2, no. 1, pp. 1177–1190, Mar. 2022.
- [15] S. Khattak, H. Nguyen, F. Mascarich, T. Dang, and K. Alexis, "Complementary multi-modal sensor fusion for resilient robot pose estimation in subterranean environments," in *Proc. Int. Conf. Unmanned Aircr. Syst. (ICUAS)*, Sep. 2020, pp. 1024–1029.
- [16] S.-K. Kim et al., "PLGRIM: Hierarchical value learning for large-scale exploration in unknown environments," in *Proc. Int. Conf. Automated Planning Scheduling*, 2021, vol. 31, no. 1, pp. 652–662.
- [17] X. Lei et al., "Early recall, late precision: Multi-robot semantic object mapping under operational constraints in perceptually-degraded environments," in *Proc. IEEE/RSJ Int. Conf. Intell. Robots Syst. (IROS)*, Oct. 2022, pp. 2017–2024.
- [18] C.-L. Lu et al., "A heterogeneous unmanned ground vehicle and blimp robot team for search and rescue using data-driven autonomy and communication-aware navigation," *Field Robot.*, vol. 2, no. 1, pp. 557–594, Mar. 2022.
- [19] Maxon Group. (2014). *Maxon DC Motor and Maxon EC Motor Key Information*. Accessed: 2020. [Online]. Available: <https://www.maxongroup.com/medias/sysmaster/root/8815460712478/DC-EC-Key-Information-14-EN-42-50.pdf>
- [20] T. Miki, J. Lee, J. Hwangbo, L. Wellhausen, V. Koltun, and M. Hutter, "Learning robust perceptive locomotion for quadrupedal robots in the wild," *Sci. Robot.*, vol. 7, no. 62, Jan. 2022, Art. no. eabk2822.
- [21] T. Moore and D. Stouch, "A generalized extended Kalman filter implementation for the robot operating system," in *Intelligent Autonomous Systems 13*, E. Menegatti, N. Michael, K. Berns, and H. Yamaguchi, Eds., Cham, Switzerland: Springer, 2016, pp. 335–348.
- [22] M. O'Brien, J. Williams, S. Chen, A. Pitt, R. Arkin, and N. Kottege, "Dynamic task allocation approaches for coordinated exploration of subterranean environments," *Auto. Robots*, vol. 47, no. 8, pp. 1559–1577, Dec. 2023.
- [23] M. Ohradzansky et al., "Multi-agent autonomy: Advancements and challenges in subterranean exploration," *Field Robot.*, vol. 2, no. 1, pp. 1068–1104, Mar. 2022.
- [24] V. Orekhov and T. Chung, "The DARPA subterranean challenge: A synopsis of the circuits stage," *Field Robot.*, vol. 2, no. 1, pp. 735–747, Mar. 2022.
- [25] M. Palieri et al., "LOCUS: A multi-sensor LiDAR-centric solution for high-precision odometry and 3D mapping in real-time," *IEEE Robot. Autom. Lett.*, vol. 6, no. 2, pp. 421–428, Apr. 2021.
- [26] J. A. Placed et al., "A survey on active simultaneous localization and mapping: State of the art and new frontiers," 2022, *arXiv:2207.00254*.
- [27] M. Ramezani et al., "Wildcat: Online continuous-time 3D LiDAR-inertial SLAM," 2022, *arXiv:2205.12595*.
- [28] D. G. Riley and E. W. Frew, "Assessment of coordinated heterogeneous exploration of complex environments," in *Proc. IEEE Conf. Control Technol. Appl. (CCTA)*, Aug. 2021, pp. 138–143.
- [29] T. Rouček et al., "System for multi-robotic exploration of underground environments CTU-CRAS-NORLAB in the DARPA subterranean challenge," *Field Robot.*, vol. 2, no. 1, pp. 1779–1818, Mar. 2022.
- [30] A. Santamaria-Navarro, R. Thakker, D. D. Fan, B. Morrell, and A.-A. Agha-Mohammadi, "Towards resilient autonomous navigation of drones," in *Robotics Research*, T. Asfour, E. Yoshida, J. Park, H. Christensen, and O. Khatib, Eds., Cham, Switzerland: Springer, 2022, pp. 922–937.
- [31] S. Scherer et al., "Resilient and modular subterranean exploration with a team of roving and flying robots," *Field Robot.*, vol. 2, no. 1, pp. 678–734, Mar. 2022.
- [32] T. Shan and B. Englot, "LeGO-LOAM: Lightweight and ground-optimized LiDAR odometry and mapping on variable terrain," in *Proc. IEEE/RSJ Int. Conf. Intell. Robots Syst. (IROS)*, Oct. 2018, pp. 4758–4765.
- [33] R. Steindl et al., "Bruce—Design and development of a dynamic hexapod robot," in *Proc. Australas. Conf. Robot. Autom. (ACRA)*, Jan. 2020, pp. 1–7.
- [34] K. Stepanas, J. Williams, E. Hernández, F. Ruetz, and T. Hines, "OHM: GPU based occupancy map generation," *IEEE Robot. Autom. Lett.*, vol. 7, no. 4, pp. 11078–11085, Oct. 2022.
- [35] B. Tam, T. Molnar, F. Talbot, B. Wood, and R. Steindl, "Deploying COTS legged robot platforms into a heterogeneous robot teams," 2021, *arXiv:2106.07182v1*.
- [36] B. Tidd, A. Cosgun, J. Leitner, and N. Hudson, "Passing through narrow gaps with deep reinforcement learning," in *Proc. IEEE/RSJ Int. Conf. Intell. Robots Syst. (IROS)*, Sep. 2021, pp. 3492–3498.
- [37] M. Tranzatto et al., "CERBERUS: Autonomous legged and aerial robotic exploration in the tunnel and urban circuits of the DARPA subterranean challenge," *Field Robot.*, vol. 2, no. 1, pp. 274–324, Mar. 2022.
- [38] M. Tranzatto et al., "CERBERUS in the DARPA subterranean challenge," *Sci. Robot.*, vol. 7, no. 66, May 2022, Art. no. eabp9742.
- [39] L. Tychsen-Smith and L. Petersson, "DeNet: Scalable real-time object detection with directed sparse sampling," in *Proc. IEEE Int. Conf. Comput. Vis. (ICCV)*, Oct. 2017, pp. 428–436.
- [40] L. Tychsen-Smith and L. Petersson, "Improving object localization with fitness NMS and bounded IoU loss," in *Proc. IEEE/CVF Conf. Comput. Vis. Pattern Recognit.*, Jun. 2018, pp. 6877–6885.
- [41] P. Vechemsky, M. Cox, P. Borges, and T. Lowe, "Colourising point clouds using independent cameras," *IEEE Robot. Autom. Lett.*, vol. 3, no. 4, pp. 3575–3582, Oct. 2018.
- [42] J. Williams et al., "Online 3D frontier-based UGV and UAV exploration using direct point cloud visibility," in *Proc. IEEE Int. Conf. Multisensor Fusion Integr. Intell. Syst. (MFI)*, Sep. 2020, pp. 263–270.
- [43] S. Zhao, H. Zhang, P. Wang, L. Nogueira, and S. Scherer, "Super odometry: IMU-centric LiDAR-visual-inertial estimator for challenging environments," in *Proc. IEEE/RSJ Int. Conf. Intell. Robots Syst. (IROS)*, Sep. 2021, pp. 8729–8736.
- [44] H. Zimmermann, "OSI reference model—The ISO model of architecture for open systems interconnection," *IEEE Trans. Commun.*, vol. C-28, no. 4, pp. 425–432, Apr. 1980.

•••